Journal of Photochemistry and Photobiology C: Photochemistry Reviews 39 (2019) 58–75

Contents lists available at ScienceDirect

Journal of Photochemistry and Photobiology C: Photochemistry Reviews

journal homepage: www.elsevier.com/locate/jphotochemrev

Recent advances in round-the-clock photocatalytic system: Mechanisms, characterization techniques and applications

Tao Cai[a,b], Yutang Liu[a,b,*], Longlu Wang[c,**], Wanyue Dong[a,b], Guangming Zeng[a,b]

[a] College of Environmental Science and Engineering, Hunan University, Lushan South Road, Yuelu District, Changsha 410082, PR China
[b] Key Laboratory of Environmental Biology and Pollution Control (Hunan University), Ministry of Education, Lushan South Road, Yuelu District, Changsha 410082, PR China
[c] School of Physics and Electronics, Hunan University, Changsha 410082, PR China

ARTICLE INFO

Article history:
Received 19 December 2018
Received in revised form 19 February 2019
Accepted 25 March 2019

Keywords:
Photocatalysis
Round-the-clock
Mechanism
Environment
Energy

ABSTRACT

Solar energy-driven semiconductor photocatalysis has gathered increasing interest in the field of energy and environmental applications. However, a vital problem that limits its application is that photocatalysis requires a continuous light source to perform redox reaction. The ability of keeping catalytic activity in the dark has been the ultimate goal for the wide application of photocatalysis. More and more efforts have been paid to develop photocatalysts to perform photocatalytic reactions under both light and dark conditions, which is so called "round-the-clock photocatalytic system" (RTCPS). RTCPS with an ability of energy storage can work well under both daytime and nighttime, which widely used in the removal of heavy metal ion, the degradation of organic pollutant, disinfection and hydrogen generation. The important potential of RTCPS necessitate timely reviews of the recent advances to streamline efforts. Thus, this review aimed to summarize the recent advances in RTCPS, including the mechanism, characterization techniques and applications. Moreover, future challenge and research direction on the mechanistic study, material design and potential applications are also discussed.

Contents

* Corresponding author at: College of Environmental Science and Engineering, Hunan University, Lushan South Road, Yuelu District, Changsha 410082, PR China.
** Corresponding author.
E-mail addresses: yt_liu@hnu.edu.cn (Y. Liu), wanglonglu@hnu.edu.cn (L. Wang).

https://doi.org/10.1016/j.jphotochemrev.2019.03.002
1389-5567/

Tao Cai is currently pursuing his Ph.D. at the College of environmental science and engineering, Hunan university. His interests include the study of solar-energy energy conversion and environmental remediation based on advanced photocatalytic nanomaterials.

Yutang Liu is a Professor at the College of environmental science and engineering, Hunan university. He obtained Ph.D from the Hunan Agricultural University. His research interests focus on synthesis and application of nanomaterials for energy conversion and environmental remediation.

Longlu Wang received his PhD degree in 2017 from Hunan University. He is currently a postdoctor at the school of physics and electronics. His current research interest is the 2D energy materials for hydrogen evolution.

Wanyue Dong is currently pursuing her Ph.D. at the College of environmental science and engineering, Hunan university. Her research interests focus on photocatalysis, including development of photocatalysts, nitrogen reduction reactions.

Guangming Zeng has been the head of the School of Environmental Science and Engineering at Hunan University since 1996. He received his Ph.D. degree from Wuhan University in 1988. He was invited as reviewers for over 50 journals and has over 320 scientific publications (journal & conference papers) with total citations at 31095 and H-index at 82. He is Highly Cited Researchers in 2017 from Clarivate Analytics. He is also the Most Cited Chinese Researchers in 2014–2017 according to Elsevier's statistics. His research interests focus on the development of novel functional materials for environmental and energy systems.

1. Introduction

The rapid development of modern industry has led to serious energy and environmental crisis [1]. Since the energy of solar radiation on earth within 1 h exceeds the total energy consumed by humans throughout the year [2], efficient utilization of solar energy could alleviate many energy and environmental pressures [3,4]. Since the discovery of Honda-Fujishima effect (photocatalytic water splitting on TiO_2) in the 1970s [5], photocatalysis has gathered increasing interest in multidisciplinary research field [6]. Photocatalysis is a complicated chemical process in which photocatalyst absorb photons energy (photons energy ($h\nu$) ≥bandgap energy (E_g) of photocatalyst) to generate electron–hole pairs, and they migrate to the surface of catalyst to initiate redox reactions [7,8]. As shown in Fig. 1a, a typical photocatalytic process involved three steps: (i) photoexcitation of semiconductor to create electron–hole pairs, (ii) separation of electron–hole pairs, and (iii) surface redox reaction. The excited carriers can undergo redox reactions with a variety of substances, such as H_2O, CO_2, O_2 and N_2, thereby widely being used in energy production [9–13] and environmental purification [14–16] (Fig. 1b).

As the name implies, the "photocatalysis" requires a continuous photo-assisted to perform redox reaction, which greatly limits its wide applications, especially at night [17]. Once illumination ceases, the generation of carriers (electron–hole pairs) within semiconductor will stopped, thereby losing their catalytic activity immediately. Therefore, there is a paradigm shift in the field of photocatalysis currently. More and more efforts have been paid to develop the photocatalyst to perform catalytic reactions under both light and dark conditions, which is so called "all-day-active photocatalyst" or "round-the-clock photocatalyst" (RTCPt) [18]. Researchers' interest began to shift from photocatalysis to "round-the-clock photocatalysis (RTCP)" [19]. RTCP is also called "memory catalysis" (MC) [20], which can maintain the catalytic activity under dark condition. The reaction system of RTCP is diverse, and the corresponding reaction mechanism is also different. In addition to the basic requirements for photocatalysis, there is another component, as the energy storage substance (ESS), is required to initiate catalytic reaction in dark [21]. ESS can store photo-generated carriers from photocatalyst under light irradiations and release these carriers in the absence of light, which is a common reaction system based on carrier storage mechanism. Briefly, electrons are excited from the valence band (VB) to the conduction band (CB) under light illumination and some of them migrate to the surface of catalyst to participate in the catalytic reactions, whereas the excess carriers are stored in ESS. Then, these stored carriers can be released to electrolyte solution to maintain catalytic activity through cathodic or anodic reactions in the dark. Therefore, this RTCP can be achieved by combining (i) a semiconductor (SC) and (ii) an ESS. The performance of this RTCP system (RTCPS) usually depends on the relative energy levels of the SC and the kinetics of the carriers processes at the interface between the SC and ESS. Some general principles to construct an efficient RTCPS are as follows: (i) For efficient electron transfer from SC to ESS, the CB of the SC should above the CB edge or Fermi level of the ESS; (ii) Good contact is required in SC-EES interface for efficient electron transfer; (iii) ESS should have the property of slowly releasing electrons in dark conditions; (iv) The CB or Fermi level position of ESS should match the redox potential of the specific reaction conditions. Additionally, it should be noted that this is not the only way to achieve RTCP. Other material system based on peroxidase mimic mechanism [22] and fluorescence-assisted mechanism [23–27], have also been reported, which will be discussed in detail in mechanism section.

Notably, RTCP with unique MC effect has boosted great interest in many applications such as removal of heavy metal ion [28–31], degradation of organic pollutant [32–38], disinfection [39–44] and hydrogen generation [19,45,46]. Considering the great potential of RTCP in practical applications, there is an urgent demand to create

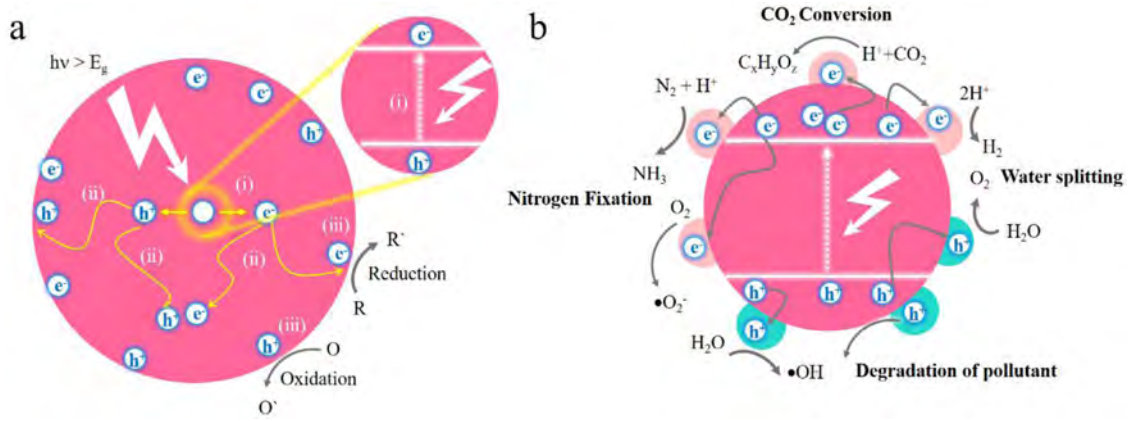

Fig. 1. (a), Photocatalytic process. (b), Photocatalytic mechanism of water splitting, degradation of pollutants, nitrogen fixation and CO_2 conversion.

a unique photocatalytic system that enables continuous operation in day and night. To favor the development of this area, it requires a deeper understanding of the mechanism of RTCP and need to develop more advanced characterization techniques. By employing these characterization techniques to gain a complete picture of the origin of observed catalytic activity.

Undoubtedly, the research about RTCP is still at its infancy stage. Their properties are still poorly understood and more potentials are largely unexploited. The important potential of this emerging field necessitate timely reviews of the recent advances to promote the development of this field. Although many excellent reviews on photocatalysis have been reported [47–51], a thorough summary and assessment on RTCP remains a gap. Therefore, the aim of this review is to summarize the state-of-the-art progresses of RTCP, describing the reaction mechanism proposed for different reaction systems, presenting the possible applications and show that how combine the experimental data and characterization techniques to analyze an existing RTCPS" as well as to design a new system. Firstly, we introduce the RTCP mechanism of different systems in detail. Secondly, we summarize various characterization techniques used in this field, in order to acquire the detail information of the nature of catalytic system. Thirdly, the applications of RTCP are also introduced. Finally, the challenges and prospects for future development of these fields are outlined.

2. Mechanism of "round-the-clock photocatalysis"

As mentioned above, the mechanism of RTCP is diverse, which depend on the kinds of catalytic system. Currently, the most common RTCPS generally composes of two kinds of materials, (i) a SC and (ii) an ESS. This catalytic system are based on the carrier storage mechanism. Besides, some materials have an peroxidase enzymatic effect, which can produce $^{\bullet}OH$ for performing catalytic reaction in the dark. Coupling a semiconductor and a long afterglow phosphor also can achieve RTCP due to the long afterglow phosphor can act as the light source in the dark. Accordingly, there are typically four kinds of catalytic system in the RTCP process, where the kinds of mechanism depend on the types of materials involved.

2.1. Electron storage mechanism

Material system such as TiO_2-WO_3 stores electrons (so called reductive energy storage) through the formation of intermediate reversible product (Equations (Eqs. (1)–(3)), [21,34,52–54] where the TiO_2 functions as a light-harvesting material and WO_3 as an electron storage material.

$$TiO_2 + h\nu \rightarrow TiO_2{*}(e^- + h^+)(carriergeneration) \quad (1)$$

$$e^-(TiO_2) \rightarrow e^-(WO_3)(interfacialelectrontransfer) \quad (2)$$

$$WO_3 + xe^- + xM^+ \rightarrow M_xWO_3(charging) \quad (3)$$

$$M_xWO_3 \rightarrow WO_3 + xe^- + xM^+(discharging) \quad (4)$$

$$e^- + O_2 \rightarrow {}^{\bullet}O_2{}^-(darkreaction) \quad (5)$$

Under light irradiation, the electron-hole pairs are generated in TiO_2 (Eq. (1)). On one hand, the holes are stayed on the surface of TiO_2, where they react with environmental medium such as adsorbed H_2O/humid air or other electrolyte. On the other hand, the excited electrons are injected to the CB of WO_3 and trapped by the intercalation of M^+ ions (M represent H^+, Li^+, Na^+, K^+, etc.) as given in Eqs. (2, 3). In absence of light, trapped electrons can be released (Eq. (4)) and reacted with electron acceptors such as O_2 (Eq. (5)). Fig. 2a illustrated the mechanism of electron storage in TiO_2-WO_3 under light illumination and release of electrons in dark. The amount of charges stored was demonstrated to be dependent on the M^+ ionic radii [55]. As shown in Fig. 2b, the charge storage capacity increased with ionic radii increased. This relationship may be related to that larger ions can stay in the structure for a longer time because the larger ionic radii limited the movement of M^+ ions. Therefore, charge storage capacity enhanced as the ionic radii increased from H^+ to K^+ (Fig. 2c).

Instead of WO_3 [56–58], other ESS have also been reported such as carbon nanotube (CNTs) [59,60], C_3N_4 [19,45,46] Ag nanoparticles (NPs) [29,61–64], Se nanorods (NRs) [65], Bi [66], MoO_3 [40], Cu_2O [67], V_2O_5 [68], polyoxometalates [54], etc. The electron storage mechanism of most of these materials is similar to WO_3, which through the formation of intermediate reversible product to trap electron. However, Ag NPs can store electrons because of its capacitive nature [62], which is different from other materials. The capacitive nature of Ag NPs impeded the charge transfer of trapped electrons out of its surface [29]. Some researchers concluded that this capacitance nature was due to the large resistance between Ag NPs and electrolyte, which slowed down the release rate of electrons [29,62]. For examples, Wood et al. [61] found that the electron transfer from ZnO to electrolytes was delayed in the presence of Ag NPs, which act as an electron storage that keeps electrons for a longer time. Since the Fermi level of Ag NPs are usually lower than the vast majority of semiconductors, Ag NPs can accumulate electrons from semiconductor such as ZnO until its Fermi level coincides with the CB edge of semiconductor, which may explain why Ag NPs can store so many electrons. Additionally, Lotsch et al. reported that C_3N_4 can store electrons through the formation of long-lived radicals. This radical species is formed with a cyanamide-functionalized polymeric network of heptazine units and can give off its trapped electrons in the dark [19]. It needs to point out that the mechanism of electron storage in some materials

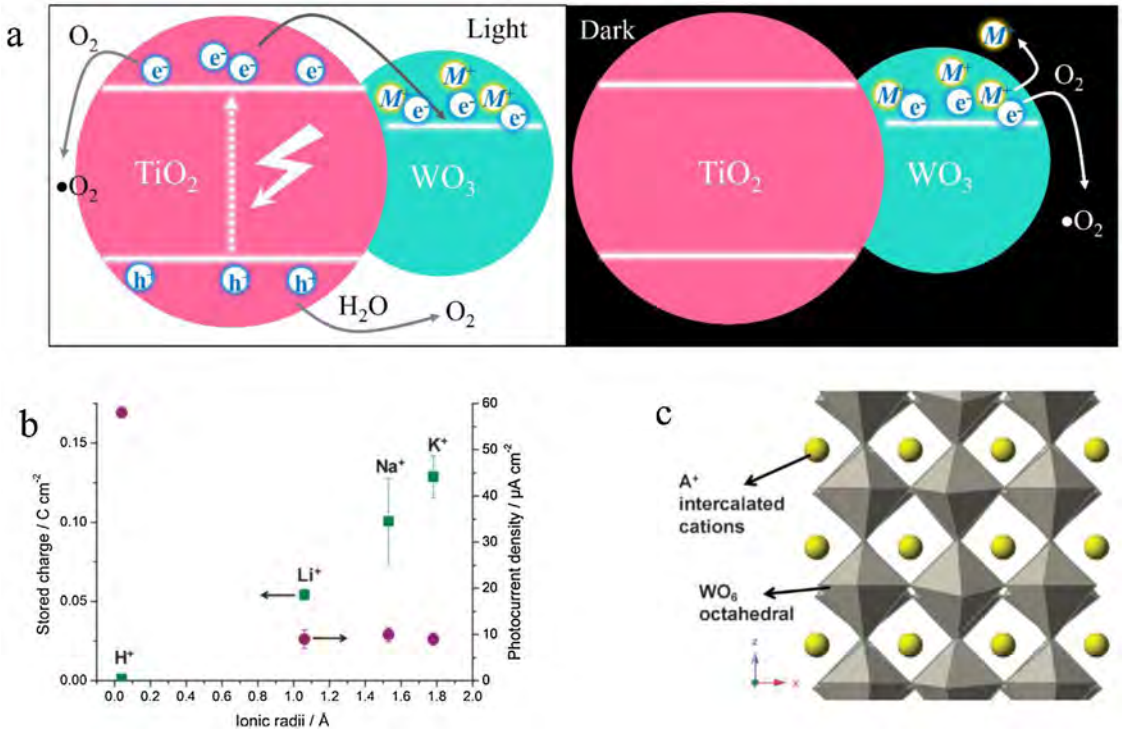

Fig. 2. (a), Electron storage mechanism in TiO_2-WO_3 system. (b), The effect of ionic radii on the amount of stored charge and the photocurrent density generated after a 10 s off-on cycle from the respectively alkali cations electrolyte. (c) Diagram showing the WO_3 crystal structure and intercalated alkali cations to illustrate the effect of ionic radii on the ability to store charges (Adapted with permission [55], Copyright 2011, Royal society of chemistry).

such as Se nanorod [65] and Bi [66] is still vague. Thus, systematic studies are encouraged to further understanding the mechanism.

2.2. Hole storage mechanism

Similar to electrons, holes can also be stored (so called oxidative energy storage). There are two models for storing holes: (i) p-n junction model and (ii) mediation model [69]. In the former, a redox-active p-type semiconductor (e.g., $Ni(OH)_2$) is combined with n-type semiconductor (e.g., TiO_2) to form a p-n junction (Fig. 3a). Under light excitation, the photogenerated holes will be transported into the bulk of $Ni(OH)_2$ through the p-n junction (Eq. (6)) and the $Ni(OH)_2$ is oxidized by holes (Eq. (7)). Photogenerated electrons will accumulated in CB of TiO_2 and be consumed by electron acceptors, such O_2 (Eq. (8)). The formed intermediate ($NiO_x(OH)_{2-x}$) can further oxidizes some substances in the dark (Eq. (9)). In this process, anion intercalation or cation (e.g., H^+) deintercalation can keeps the electrically neutral of system (Eq. (7)), thereby stabilizing retention of oxidative energy.

$$TiO_2{*}(h^+) \rightarrow Ni(OH)_2(h^+) \quad (6)$$

$$Ni(OH)_2 + xh^+ + xOH^- \rightarrow NiO_x(OH)_{2-x} + xH_2O \quad (7)$$

$$O_2 + 2H^+ + 2e^- \rightarrow H_2O_2 \quad (8)$$

$$NiO_x(OH)_{2-x} + \text{substance} \rightarrow Ni(OH)_2 + \text{products} \quad (9)$$

In the latter, the mediation model (Fig. 3b), an electron mediator such as Fe^{3+}/Fe^{2+} redox couple was introduced. Photogenerated electrons in $Ni(OH)_2$ could be efficient transported into the CB of TiO_2 through electron mediator. The remaining photogenerated holes in the VB of $Ni(OH)_2$ will oxidize itself (Eq. (7)), thereby storing oxidative energy. It should mention that both p-n junction model and mediation model are beneficial to carrier separation because p-n junction could provide built-in electric field and electron mediator could induce high-speed electron transfer. Thus, hole storage efficiency will improved due to reduce the loss resulting from carrier recombination. This hole storage mechanism was usually found in TiO_2-$Ni(OH)_2$ system [69–72], TiO_2-NiO system [73,74], and $TiO_2/SiO_2/MnO_x$ system [75]. Notably, the hole storage efficiency of this system is smaller than electron storage efficiency of electron storage system (TiO_2-WO_3). This is possibly due to the loss of holes by adsorbed water oxidization or re-reduction of $Ni(OH)_2$ by photogenerated electrons [18] In addition, it was also demonstrated that the hole storage efficiency can be enhanced in p-n junction model by increasing the junction area (e.g., making the TiO_2 into porous structure).

2.3. Peroxidase mimic mechanism

Natural peroxidases (e.g., horseradish peroxidase) are usually used as catalysts in enzyme-linked immunosorbent assays [76]. In the presence of an oxidant such as hydrogen peroxide (H_2O_2), peroxidase can oxidize chromogenic substrates (e.g., 3,3,5,5-tetramethylbenzidine, TMB) into colored molecules [77–82]. In fact, except for horseradish peroxidase, there are other catalysts can oxidize the TMB in the presence of H_2O_2. Some metal-oxide or metal NPs such as Pt NPs [76,83], $ZnFe_2O_4$ NPs [84], and Au NPs [22,82,85] have recently been demonstrated to have intrinsic peroxidase mimetic nature similar to natural peroxidases. Possible reaction mechanism for the TMB–H_2O_2–Pt system were showed in Fig. 4a [76]. Firstly, Pt NPs catalyze the production of •OH radical, which assumed that the O—O bond of H_2O_2 is rapidly destroyed by the catalytic action of Pt NPs [76,83]. Then, the producing $^{\bullet}$OH radicals were stabilized on the surface of the Pt NPs and subsequently react with TMB [86]. Since the reaction process is based on the radical chain mechanism, this catalytic system can be introduced into the field of RTCP. Hsu et al. showed that Au@Cu_7S_4 yolk@shell nanocrystal-decorated TiO_2 nanowires could perform efficient methyl orange (MO) degradation under both light and dark condition [22]. Such a capability was ascribed to

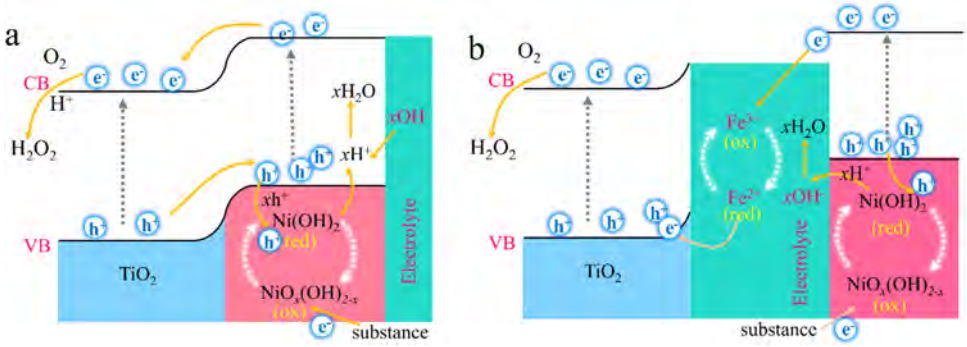

Fig. 3. Oxidative energy storage through (a) the p–n junction model and (b) mediator model.

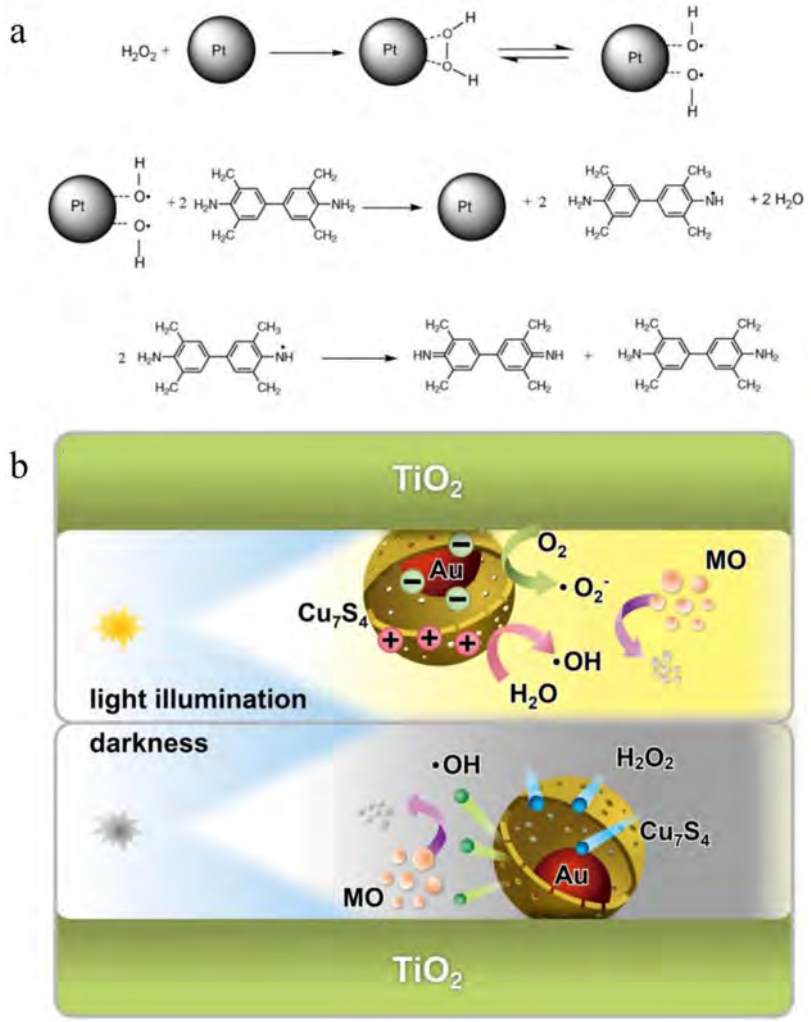

Fig. 4. (a), Possible mechanism for the TMB–H_2O_2–Pt colloid system (Adapted with permission [76], Copyright 2011, Elsevier). (b), Schematic illustration of the coupling of photocatalysis and peroxidase mimics on TiO_2-Au@Cu_7S_4 (Adapted with permission [22], Copyright 2017, Elsevier).

the peroxidase function of Au, which triggered the production of $^{\bullet}OH$ radicals for proceeding pollutant degradation in dark environment (Fig. 4b). Thus, an all-day-active photocatalyst model was established by employing Au@Cu_7S_4 yolk@shell nanocrystal decorated TiO_2 nanowires. It should point out that the "dark reaction" requires the participation of H_2O_2, which is similar to photo-Fenton reaction. However, unlike the photo-Fenton catalytic system, the TiO_2-Au@Cu_7S_4 can work continuously during daytime and nighttime, which is very valuable for the practical application of environmental cleaning.

2.4. Fluorescence-assisted mechanism

Recently, some studies have been reported to combine photocatalyst with long afterglow phosphors that can be excited by light irradiated, thereby emitting long lasting phosphorescence in the dark to excite photocatalyst and achieve persistent photocatalysis [23,87–90]. The mechanism of the persistent luminescence in $Sr_2MgSi_2O_7$: (Eu, Dy)/g-C_3N_4 system was proposed and showed in Fig. 5 [17]. When the phosphor was illuminated by light, the charge energy was transferred to the $4f^7$ ground state of Eu^{2+} (arrow

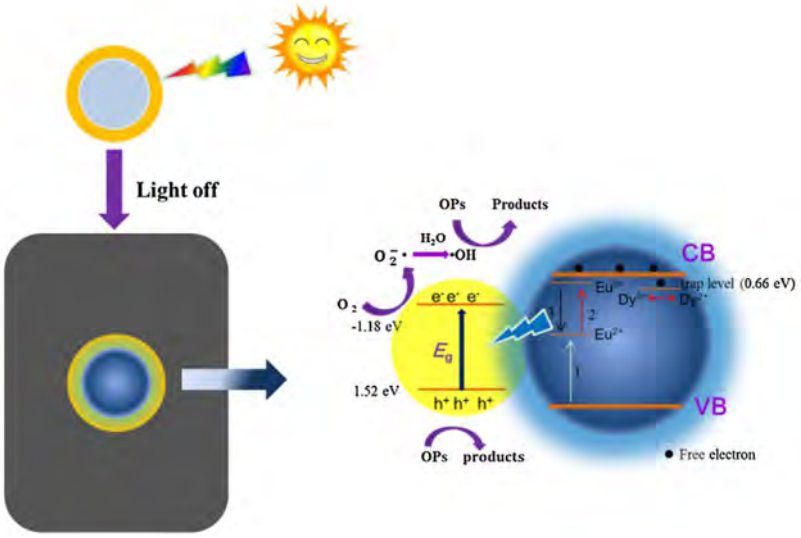

Fig. 5. Schematic illustration of the charge transfer in $Sr_2MgSi_2O_7$: (Eu, Dy)/g-C_3N_4 (Adapted with permission [17], Copyright 2016, Elsevier).

1) and Eu^{2+} was excited to the $4f^65d$ state located within the CB (arrow 2). Autoionization generated a free electron and Eu^{3+} was left. Dy^{3+} captured the electron to form Dy^{2+} with a ground state below the bottom of the CB. Once illumination stopped, the electron will transfer from Dy^{2+} back to the CB and then recombined with Eu^{3+}, resulting in 5d-4f emission because of the thermally activated release (arrow 3). The g-C_3N_4 could be excited by the fluorescence and then created photogenerated carriers. The electrons subsequently transferred to the surface of the catalyst and react with H_2O and O_2 to generate $^{\bullet}OH$ and $^{\bullet}O_2^-$. Such a fluorescence-assisted system enables persistent photocatalysis in day and night and can be expanded to other field.

3. Characterization techniques

To clearly depict the mechanism of RTCP, it is necessary to probe the behaviors of carrier storage and release through some characterization techniques. To date, many characterization methods have been developed to study the behaviors of electron storage and discharge in RTCPS. In this section, we will discuss these characterization methods and their basic principles in conjunction with specific examples. It should be noted that the characterization methods of other RTCPS (e.g., hole storage system, peroxidase mimic system, etc.) are ignored because the current mainstream of RTCPS is based on electron storage mechanisms.

3.1. Electron storage behavior characterizations

As mentioned above, In TiO_2-WO_3 system electron can be stored in WO_3 by the formation of intermediate reversible product (e.g., H_xWO_3), which is known as electrochromism/photochromism. The obvious change of the color can be observed when the formation of H_xWO_3 during charge process (Fig. 6a) [91]. Being charged, a composition sample of H_xWO_3/WO_3 appeared. The UV–vis–NIR diffuse reflectance spectra (DRS) of the WO_3 and H_xWO_3/WO_3 can be used to test their optical properties. As shown in Fig. 6b, the absorbance of H_xWO_3/WO_3 increases significantly in the wavelength range of 480–2000 nm, which is in accordance with the color changes from yellow (WO_3) to green (H_xWO_3/WO_3) [92]. It is generally believed that the change of WO_3 electronic structure caused the its variable light absorption, which is concerned with the oxidation state of W atom (e.g., from W^{6+} to W^{5+}) [93,94]. Thus, the generation of low valence W species in H_xWO_3 contributes to the near-infrared light absorption. In addition, Shang et al. reported that atomic force microscopy (AFM) can be used to examine the surface charge distribution of the nitrogen-doped titanium oxide (TiON)/PdO film, which was carried out in the contact mode when the TiON/PdO film was illumined [95]. Fig. 6c revealed the electric current distribution on the surface of TiON/PdO thin film under light irradiation without additional electric voltage required. The picture was generated by superimposing the current profile on the 3D image of the height profile created by the MFP-3D software (Asylum Research). The 3D height picture showed the morphological structure and the yellow color presented the current value on the material surface. Most parts of the material surface is red color, while some bright yellow spots were found among the grain boundary areas, where PdO NPs were distributed in these areas, indicating an accumulation of electrons on PdO NPs. The in-situ X-ray photoelectron spectroscopy (XPS) analysis can be used to investigate the changes in the valence states of elements. There was an obvious difference in the Pd 3d peak position and shape with or without illumination (Fig. 6d). Under dark condition, the Pd 3d5/2 peak at 336.20 eV was assigned to the PdO. However, under light irradiation, Pd 3d peaks were widen and the peak of Pd 3d5/2 was shifted to 335.30 eV, which can be attributed to the combination of Pd^{2+} 3d5/2 (peak at 336.2 eV) and Pd° 3d5/2 (peak at 335.2 eV). The result clearly demonstrated that some PdO NPs have been reduced to metallic Pd° under visible-light irradiation because of the electron accumulation. When the light was turned off, the Pd 3d peak return to the original location, indicating the discharge process.

It should mention that in-situ characterization of the carrier transfer during the storing process remain challenging. There are limited literature on this carrier transfer process. Recently, Li et al. developed a surface photovoltage microscopy (SPVM) method to image the diffused carrier separation process on a high-symmetry Cu_2O photocatalyst particle [96]. SPVM mainly include light system, Kelvin probe force microscopy (KPFM) and nanometre-resolution surface photovoltage (SPV) (Fig. 7a). SPVM showed an obvious spatial correlation between the charge distribution and illumination distribution (Fig. 7b). Photogenerated holes (positive SPV, purple region) were imaged in the illuminated region, whereas photogenerated electrons (negative SPV, red region) were imaged in the shadow region. Authors investigated the effect of irradiation asymmetry on this charge transfer process. SPVM images of a single Cu_2O particle photoexcited with increasing laser intensity (Fig. 7b_1–b_6) showed that the photogenerated

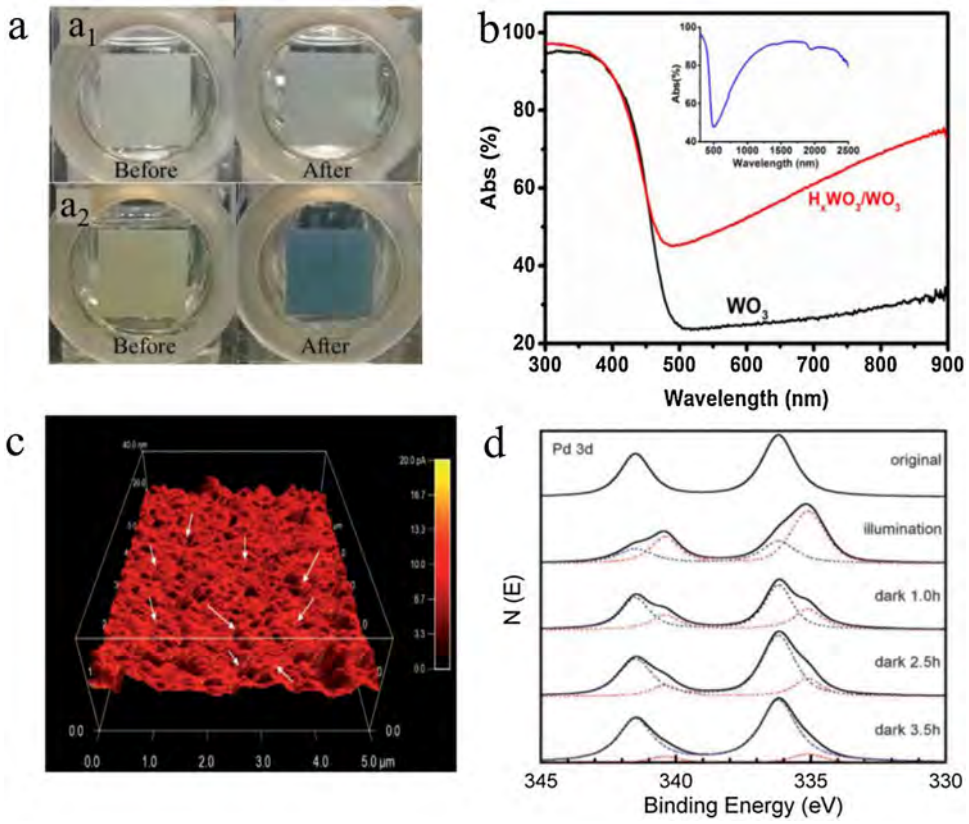

Fig. 6. (a), Appearance of hybrid WO_3/TiO_2 electrodes with WO_3 loadings of (a_1) 1 wt % and (a_2) 6 wt % before and after charging (Adapted with permission [91], Copyright 2015, American Chemical Society). (b), UV–vis diffuse reflectance spectra of WO_3 and H_xWO_3/WO_3 (Adapted with permission [92], Copyright 2015, Elsevier). (c), AFM 3D height image with the yellow-hot color displaying the electric current value of the TiON/PdO thin film surface under visible light illumination. (Note that white arrows point out some places with stronger electric current signal in dispersed spots on the surface to guide eyes). (d), In situ XPS high-resolution scans over Pd 3d peaks on TiON/PdO thin film originally in the dark for 5 h, under visible light illumination, and in a dark environment for 1 h, 2.5 h and 3.5 h after the visible light is off (Adapted with permission [95], Copyright 2010, Royal society of chemistry).

electrons on the shadow facet disappeared and changed to holes. SPVM method can monitor the photovoltage of the material surface in time and image it in different areas. Thus, using this method can clearly observe the charge transfer process, which has a great potential applied for in-situ characterization of the electron/hole transfer.

In a sum, electron storage behavior can be characterized by following method as: (i) Color change and spectroscopy characterization; (ii) AFM; (iii) In-situ XPS; (iv) SPVM. It is worth noting that a single characterization method does not fully reflect the real situation of electronic storage. It is necessary to combine multiple characterization methods to analyze and understand the storage behavior of electrons. Moreover, there are some other characterization methods that can be used, such as electrochemical characterization, etc. The development of new characterization method is encouraged to better understanding electron storage process.

3.2. Electron storage capacity characterizations

The electron storage capacity can be measured by potentiometry in discharge process (Eq. (10)).

$$Q = I \times t \tag{10}$$

where Q, I and t are quantity of electric charge, current and time, respectively. Fujishima et al. measure the amount of electrons accumulated in the TiO_2–WO_3 film by potentiometry at 2 mA cm^{-2} (cut-off potential −0.1 V vs. Ag/AgCl) after light irradiation. [52] The discharge time increases as the UV irradiation time increases until the maximum was reached (Fig. 8a). Thus, discharge capacity was calculated to be 3.7 mC cm^{-2} [= 2 (μA cm^{-2}) × 31(min) × 60/1000]. Moreover, electron storage capacity could be titrated with electron acceptors such as methylene blue (MB), [62] C_{60} [97], CNTs [59], or graphene oxide (GO) [98]. For example, Kamat et al. measured the capacity of electrons in TiO_2/Ag system by MB titration. [62] MB with an absorption at 655 nm can be reduced into MB^{2-}, a leuco dye, by discharged electrons (Eqs. (11) and (12)).

$$TiO_2/Ag(e^-) + MB \rightarrow TiO_2/Ag + MB^{-\bullet} \tag{11}$$

$$2MB^{-\bullet} \rightarrow MB^{2-} + MB \tag{12}$$

MB with a fixed increments was added dropwise into the previously irradiated TiO_2/Ag suspension under N_2 atmosphere. Since the MB^{2-} is a colorless dye, any absorption at 655 nm could not be observed (Fig. 8b). As continued addition of MB, the electrons in TiO_2/Ag system are exhausted. When all of the stored electrons are depleted form TiO_2/Ag system, further addition of MB will cause an obvious absorption at 655 nm (Fig. 8c). Therefore, electron storage capacity can be calculated by Eqs. (11) and (12).

Some other special methods also can be used to estimate the electron storage capacity. For example, Reisner et al. got the electron storage capacity by the amount of hydrogen production in the dark (assume that all stored electrons are used to generate hydrogen) [45]. Zhao group reported that the electron storage capacity can be obtained by the amount of heavy metal ion consumption (assume that all stored electrons are used to reduce heavy metal ion) [28]. It should be pointed out that these methods are only suitable for specific reactions and are not universal. The accuracy of

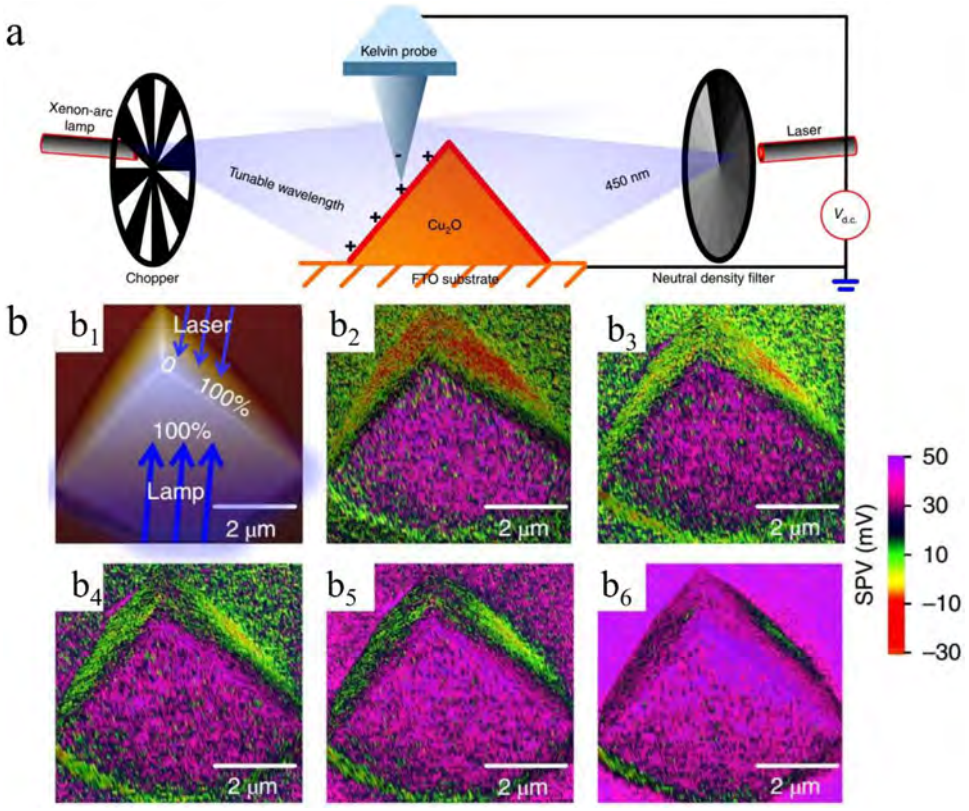

Fig. 7. (a) Experimental set-up for SPV imaging of the Cu_2O photocatalyst. Two light sources with a tunable light intensity and opposite irradiation direction were employed to perform the asymmetric photoexcitation. (b) Impact of illumination symmetry on the charge separation. (b_1) AFM image of a Cu_2O particle. (b_2-b_6), The corresponding SPVM images of the same particle under dual light irradiation. The laser intensity is tuned to 0% (b_2), 10% (b_3), 20% (b_4), 40% (b_5) and 100% (b_6) of the lamp intensity. (Adapted with permission [96], Copyright 2018, Nature publishing group).

these methods needs to be improved because it is based on the hypothesis that all electrons are used for specific reactions. Therefore, further study is necessary to develop new methods to precise calculate the actual electron storage capacity.

3.3. Discharge behavior characterizations

Most electron storage materials have similar electrochromism/photochromism phenomenon. So the discharge behavior can be confirmed by color observation and the characterization of spectrophotometry. Reisner et al. reported that photoexcited $^{NCN}CN_x$ in the presence of an organic substrate can accumulate ultralong-lived "trapped electrons", which allow for H_2 generation in the dark [45]. NiP was added to the pre-irradiated $^{NCN}CN_x$ suspension (blue color) under N_2 atmosphere, and the spectrophotometry was employed to monitor the absorption peak (λ = 650 nm) in the dark (Fig. 9a). A obvious decrease in the absorption peak at λ = 650 nm was observed, indicating the discharge process (trapped electrons were transferred from $^{NCN}CN_x$ to NiP). The absorption peak was disappeared completely after 30 min and the color of the suspension converted back into yellow (the original color of $^{NCN}CN_x$). When adding a NiP-free phosphate (KPi) aqueous solution into another blue $^{NCN}CN_x$ suspension, the color of solution remained blue and no obvious change can be observed in the absorption spectra. Thus, the changes of the color and absorption spectra is caused by the discharge behavior in the presence of electron acceptor (NiP). Meanwhile, H_2 evolution was observed only in $^{NCN}CN_x$-NiP system in the dark (Fig. 9b), which further demonstrated the transfer of the trapped electrons from $^{NCN}CN_x$ to NiP (cocatalyst). In addition, photoelectrochemical measurements also can employed to verify this discharge behavior. The open circuit potential (OCP) was used to monitor the discharge phenomenon. [19] The OCP of $^{NCN}CN_x$ increased to approximately -500 mV vs NHE under irradiation, and declined to its original state after the light was turned off (Fig. 9c). This phenomenon can be reproduced for more than 10 cycles without obvious changes. When increasing the illumination time, the time required for the blue state to decay back to the yellow state also increased (Fig. 9d). This behavior indicated $^{NCN}CN_x$ has a resembles capacitive charging and discharging. When the light is turned off, the decay of the photovoltage of the irradiated electrodes of TiO_2, Pt/TiO_2, and Ag/TiO_2 was used to monitor the slow discharge of electrons, which reported by Choi et al. [29] Compared with TiO_2 and Pt/TiO_2 electrodes, the postirradiation photovoltage on the Ag/TiO_2 electrode was obvious delayed (Fig. 9e). Since storage electron can be released and react with O_2 to produce radical, ESR also can be used to detect the formation of radical in the dark. For the irradiated Se NRs, a number of photogenerated carriers were produced and transfer to the surfaces of Se NRs to participate in $^{\bullet}OH$ generation. After stopping the irradiation, a considerable number of carriers may still remain, providing excess •OH supply in the dark to alleviate the decay of DMPO–$^{\bullet}OH$ (Fig. 9f) [65].

The released electrons react with various electron acceptors (e.g., O_2, H^+, etc.) during "dark reaction" period. Thus, in fact, how many electrons participate in the reaction of the target is uncertain because of the complexity of the environmental medium. It is not precise that simply describing or calculating the amount of electrons by the amount of final product (e.g., the amount of H_2). Therefore, how to accurately describe the release behavior of electrons and the final destination is the future research direction. The development of new characterization technique to insight into the discharge behavior is also recommend.

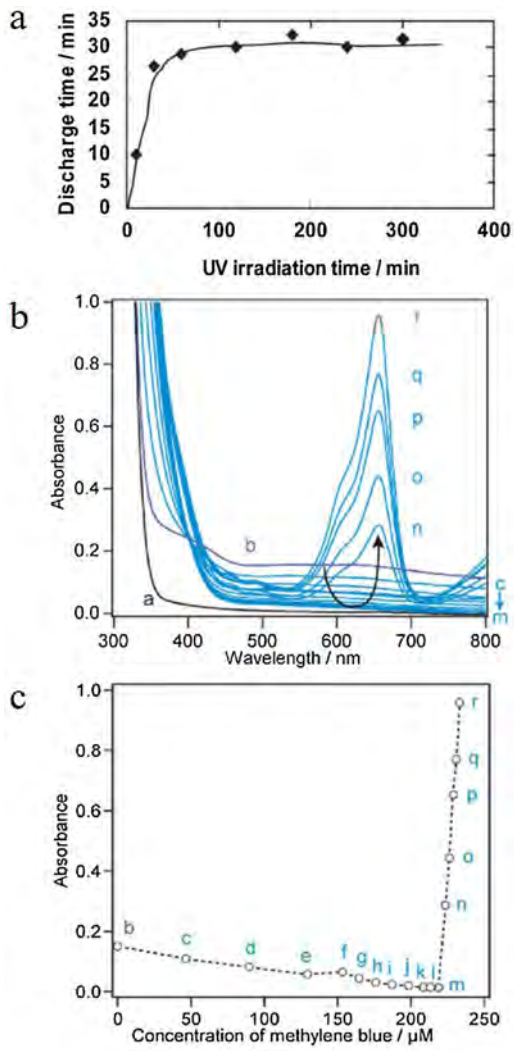

Fig. 8. (a) The relationship between the discharge time (at 2 μA cm^{-2} in NaCl solution, cut-off potential = −0.1 V vs. Ag/AgCl) and the UV irradiation time (Adapted with permission [52], Copyright 2003, Royal society of chemistry). (b) Absorption spectra of TiO_2 colloidal solution (5.8 mM) and $AgNO_3$ (8.6 μM) "a" before and "b" after irradiated solution saturated with N_2. The blue colored spectra "c-r" were recorded following incremental addition of MB to the suspension corresponding to "b" under N_2 atmosphere. (c) Titrations of stored electrons as measured from the changes in absorbance at 655 nm plotted are versus MB concentration (Adapted with permission [62], Copyright 2011, American Chemical Society).

4. Applications

The TiO_2-WO_3 system was developed by Akira Fujishima, et al. in 2001 for the anticorrosion applications firstly under both light and dark conditions [21]. To date, on the one hand, various RTCPS have been investigated by many scholars. On the other hand, many potential applications involving the field of environmental and energy were emerged. In this section, we will summarize the main applications of various RTCPS recently. Moreover, the challenges and potential applications in future are also mentioned.

4.1. Removal of heavy metal ion

Efficient reduction of heavy metal ions (e.g., Cr^{6+}, Hg^{2+}, and Ag^{+} et. al.) in dark have been achieved in TiO_2-WO_3 system [28]. WO_3-TiO_2 can store electrons under UV light irradiation even in the presence of O_2 and these stored electrons can be released to reduce heavy metal ions. This study substantially revealed that toxic heavy metal ions were good electron acceptor, which can be reduced easily by the trapped electrons in TiO_2-WO_3 system. It is need noted that O_2 as the electron sacrificial agent can inhibit the storage of electrons. However, the electrons reacted with O_2 can generate some reactive oxygen species (ROS) such as $^{\bullet}O_2^{-}$, which can be applied to the degradation process. Thus, the charging process should try to avoid the presence of O_2, while the discharging process can utilize O_2 to produce ROS for environmental cleaning.

A recent study has shown an interesting application of this RTCPS, which is a sequential process combination of photocatalytic oxidation and dark reduction [29]. Choi group demonstrated a sequential process of photocatalysis-dark reaction, wherein 4-chlorophenol (4-CP) were degraded on Ag/TiO_2 under UV light illumination and the reduction of Cr^{6+} in the dark was subsequently followed (Fig. 10). During the photocatalytic reaction period, photogenerated electrons were stored in Ag NPs while photogenerated holes performed the degradation of 4-CP. In the dark reaction period, the trapped electrons in Ag NPs coupled with the reaction intermediates were used to reduce Cr^{6+} (Fig. 10). The idea of not only using the photocatalytic reaction period (daytime) but also the dark reduction period (night time) for environmental remediation could be an interesting strategy. In addition, a spontaneous reduction of Cr^{6+} was also observed on In_5nS_2 [30] and Ti_3C_2 [99] under dark condition.

4.2. Degradation of pollutant

The first example that applied to the RTCP degradation was reported in TiO_2-$Ni(OH)_2$ system [69]. The holes (oxidative energy) stored in the TiO_2–$Ni(OH)_2$ bilayer film under light irradiation can be used to oxidize various species such as phenol, aldehydes, formate and alcohols in the dark. It was demonstrated that these species were probably oxidized by the $NiO_x(OH)_{2-x}$ (the oxidized state of $Ni(OH)_2$) because of the storage of oxidative energy. The mechanism is as follows (Eqs. (13)–(15)):

$$NiO_x(OH)_{2-x} + xH_2O + xe^- \leftrightarrow Ni(OH)_2 + xOH^- \quad (13)$$

$$CH_3OH + 6\,h^+ + 6OH^- \rightarrow CO_2 + 5H_2O \quad (14)$$

$$HCHO + 4\,h^+ + 4OH^- \rightarrow CO_2 + 3H_2O \quad (15)$$

In addition, the dark catalytic activity of TiON/PdO system was investigated on the degradation of MB dye [20]. TiON/PdO sample was firstly illuminated for about 10 h to simulate the daytime sunlight irradiation. As a control, another TiON/PdO sample only kept in dark. After the light source was removed off, the dark reaction between MB and TiON/PdO was studied. As the reaction time increase, the adsorption process gradually achieved the equilibrium (about 2 h), and no obvious change of MB residual concentration can be observed in TiON/PdO without prior illumination. Interestingly, further decrease of the MB residual concentration was observed in TiON/PdO with prior illumination (Fig. 11a). This results demonstrated that the degradation of residual MB stem from catalytic "memory" effect not the adsorption. Se NRs have also been reported to possess the dark catalytic activity toward MB [65]. In another report, platinized semiconductor particles ($Pt–HCa_2Nb_3O_{10}$) can catalyze room temperature air oxidation of MO without light [32]. The WO_3/TiO_2 microspheres were prepared and investigated for the degradation of MO in dark [34]. It was found that the WO_3/TiO_2 hollow microsphere composites showed the excellent degradation efficiency (22%) in dark after exposure to visible light for a period of time.

For another example, a g-C_3N_4/CNTs/graphene (CN-CNT-Gr) photocatalyst was studied on the degradation of phenol [38]. Fig. 11b showed the degradation of phenol by the g-C_3N_4 sample and different CN-CNT-Gr samples (CN-CNT-Gr^1, CN-CNT-Gr^2 and CN-CNT-Gr^3, which represent mass ratio of g-C_3N_4 : CNT-Gr are 1:1,

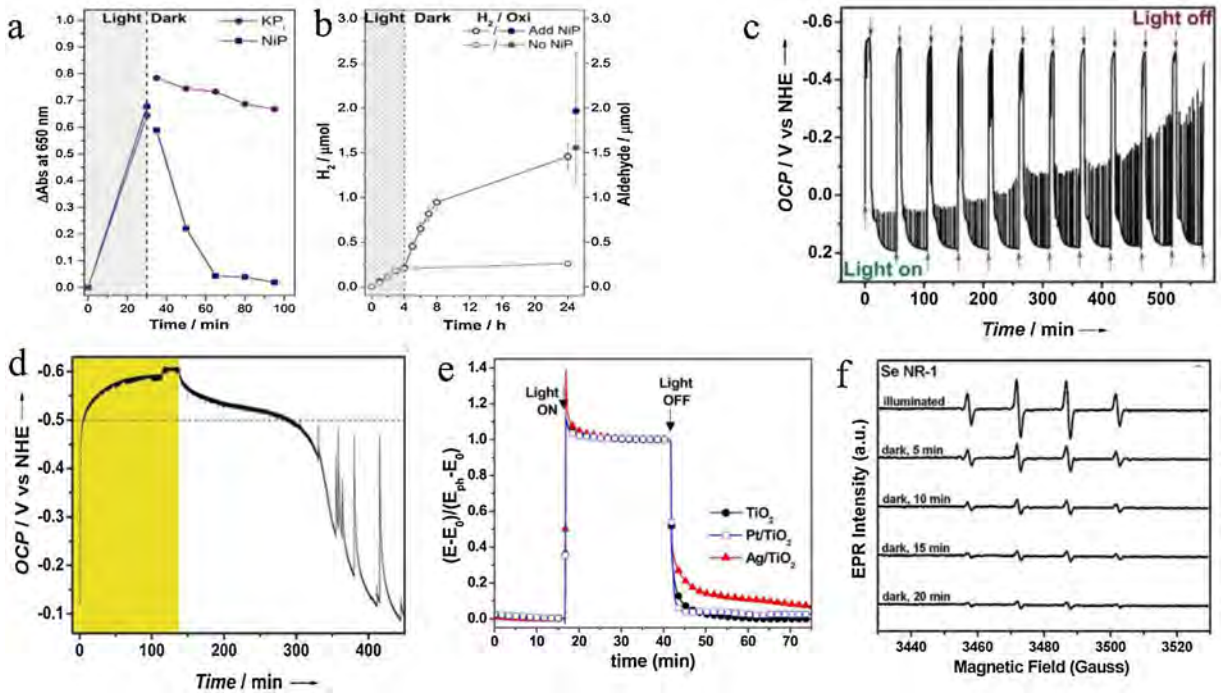

Fig. 9. (a) Spectrophotometry of the appearance (during irradiation) and disappearance (upon addition of NiP in the dark) of photoexcited electrons in $^{NCN}CN_x$ at λ = 650 nm. (b) Two photoreactors were prepared with $^{NCN}CN_x$ (5 mg) and 4-MBA (30 μmol) in the absence of NiP in an aqueous KPi solution (0.02 M, pH 4.5, 3 mL) and irradiated with 1 sun irradiation (AM 1.5 G, 25 °C) (Adapted with permission [45], Copyright 2016, American Chemical Society). (c) OCP monitored under continuous chopped light, showing reproducible excitation of the blue state at about 500 mV versus NHE. (d) Effect of longer illumination time in the presence of sodium citrate as electron donor (period of illumination highlighted in yellow) (Adapted with permission [19], Copyright 2017, Wiley). (e) Time profiles of the normalized OCP of the bare TiO_2, Pt/TiO_2, and Ag/TiO_2 electrode before, during, and after UV irradiation (Adapted with permission [29], Copyright 2017, American Chemical Society). (f) Time evolution of DMPO–$^{\bullet}$OH EPR spectrum in the dark for Se NRs (Adapted with permission [65], Copyright 2011, Elsevier).

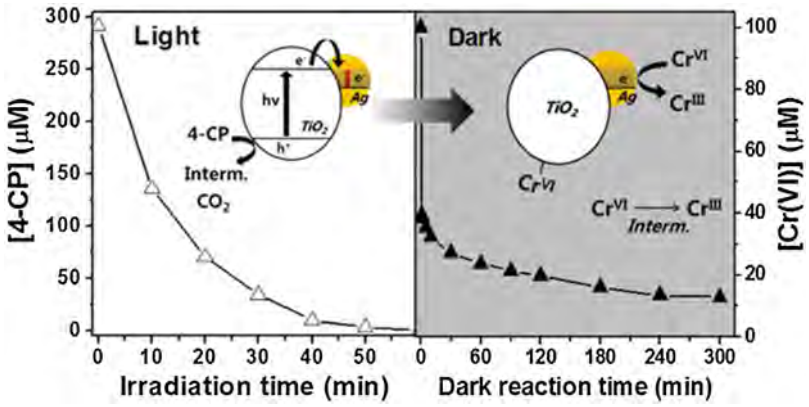

Fig. 10. The mechanism of photocatalytic degradation of 4-CP and the following reductive removal of Cr^{6+} in the dark (Adapted with permission [29], Copyright 2017, American Chemical Society).

2:3 and 1:2, respectively.) after 5 h irradiation. No obvious postirradiation catalytic effect was observed for the g-C_3N_4 sample under dark condition. The postirradiation catalytic effect of CN-CNT-Gr was improved with the addition of g-C_3N_4 compared with the simple g-C_3N_4. The removal efficiency of CN-CNT-Gr[2] catalyst toward the degradation of phenol with 5 h was about 25.3%, which was 1.1 and 1.2 times greater than that of CN-CNT-Gr[3] (22.9%) and CN-CNT-Gr[1] (20.6%), respectively. However, the postirradiation catalytic effect was greatly inhibited with the addition of $AgNO_3$ (Fig. 11c). This experimental result demonstrated that stored electrons were the vital active species in the degradation of phenol without irradiation. They proposed the catalytic mechanism according to the experimental result (Fig. 11d). First, under visible light illumination, the layer g-C_3N_4 can be excited to generate photogenerated electrons in the CB of g-C_3N_4. Next, these photogenerated electrons can further transfer to the surface of CNT-Gr and easily react with O_2 to generate $^{\bullet}O_2^-$. In addition, a part of electrons would captured and stored by the CNT-Gr. When the light source was removed out, these captured photoelectrons were released to the surface of catalyst again, where they can participate in the production of $^{\bullet}$OH radicals through interaction with O_2 and H_2O. It should be pointed out that electron can be stored in CNT-Gr because they are often used as supercapacitors due to their high electron-storage capacities and good electrical conductivity [100]. Supercapacitors store the electron via two operating mechanisms including electrochemical double-layer capacitance (EDLC) and pseudo-capacitance [101]. It was reported that CNT are characteristic of both the EDLC and the pseudo-capacitance. For a detailed description of the mech-

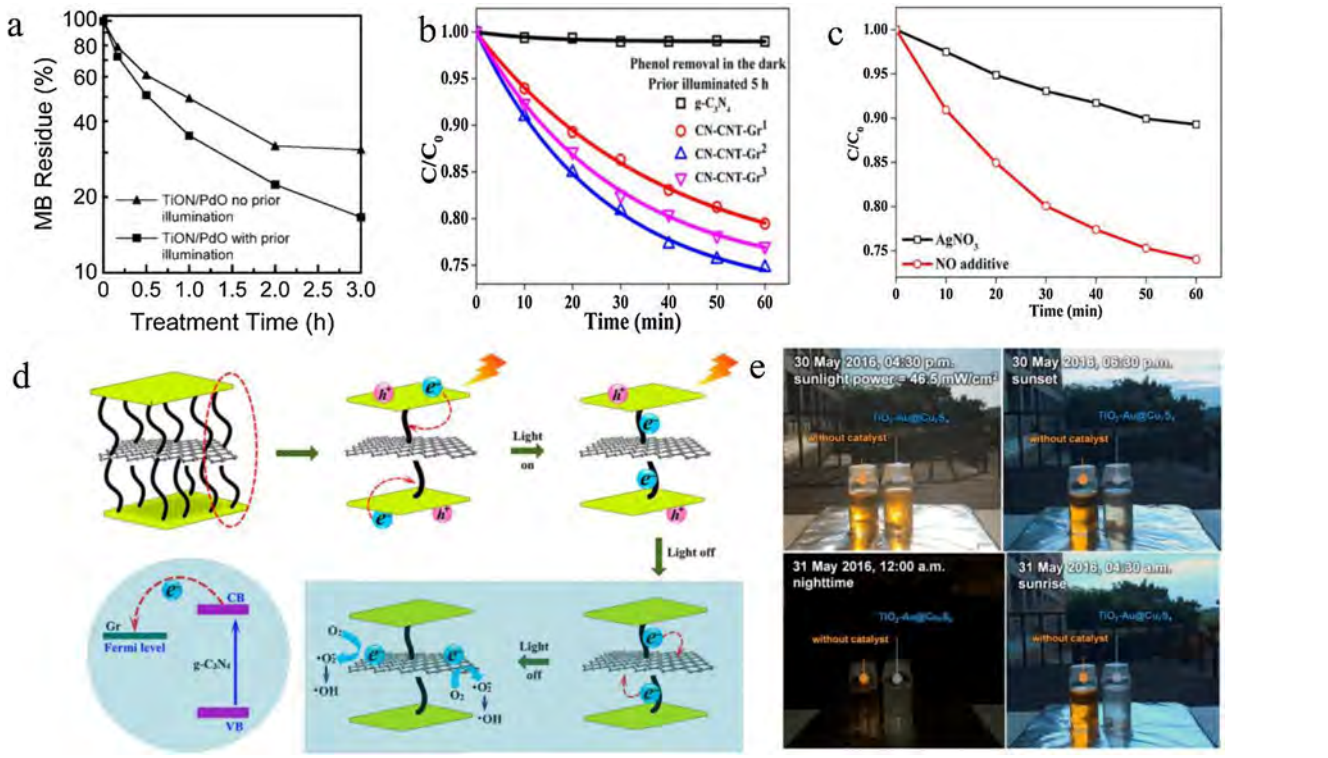

Fig. 11. (a) MB residue percentage versus treatment time with TiON/PdO fibers (Adapted with permission [20], Copyright 2008, Weliy). (b) Phenol (C_0 = 5 mg L^{-1}) removal in the dark with g-C_3N_4 and different CN-CNT-Gr samples after prior illumination for 5 h. (c) Phenol removal in the dark with CN-CNT-Gr^2 that was illuminated for 5 h upon the addition of $AgNO_3$. (d) Schematic diagram illustrating the removal of phenol in the dark by the CN-CNT-Gr^2 catalyst illuminated for 5 h (Adapted with permission [38], Copyright 2017, American Chemical Society). (e) Demonstration of using TiO_2-Au@Cu_7S_4 as an all-day-active photocatalyst for MO degradation. The controlled experiment without catalyst addition was also conducted for comparison (Adapted with permission [22], Copyright 2017, Elsevier).

anism of electron storage by CNT, the readers can refer to the reference in the field of supercapacitors [101].

Recently, Hsu et al. reported that Au@Cu_7S_4 yolk@shell nanocrystal-decorated TiO_2 nanowires (TiO_2-Au@Cu_7S_4) were capable of performing efficient MO degradation in whole day [22]. Firstly, the degradation of MO was performed in sunlight (04:30 p.m. local time). With the arrival of the nighttime (06:30 p.m. local time), the MO residual concentration further decrease when adding H_2O_2 into reaction solution. In the daytime, approximately 76% of MO was removed by the photocatalytic degradation of TiO_2-Au@Cu_7S_4. Then, the peroxidase mimic effect of Au NPs work at night, and the residual MO was completely degraded before the sun rose next morning (Fig. 11e).

4.3. Disinfection

TiO_2-WO_3 system was also used to bactericidal disinfections [39]. The discovery of TiO_2-WO_3 for such antimicrobial applications has been fundamentally helpful in understanding their possible mechanisms of their photocatalytic activity under dark conditions. TiO_2-WO_3 photocatalyst films can be charged under UV light irradiation. When exposure in dark about 6 h, These films still displayed a decent bactericidal effect against *Escherichia coli* (*E. coli*). Experimental studies showed that the observed origin of the antibacterial activity of TiO_2-WO_3 films was mainly stem from the production of $^{\bullet}HO_2$ and H_2O_2 generated by the reaction between the released electrons and O_2 in the dark.

Generally speaking, the disinfection ability of semiconductors arise from the photo-generated carriers. The interreact can be happened directly between the bacterial membrane lipids and holes, or by the generation of $^{\bullet}OH$ indirectly (such as reacting with the OH^-) to perform chemical transformations on the biomolecules [102]. The produced electrons can be scavenged by electron acceptor in surrounding environmental media (e.g., H^+) [103]. However, all of these reactions can only occur under light conditions. Interestingly, Liu et al. found that Ag NPs/TiO_2 coatings (TOC) can still remain the bactericidal effect in the dark [63]. The excellent bactericidal effect is highly related to the stronger electron storage capability of Ag NPs, which can induce accumulation of adequate holes on TOC, arousing oxidation reactions to bacterial cells in the dark. The mechanism was shown in Fig. 12a. A "bacterial charging" process can happen in the dark (Electrons produced by bacteria can be transferred into the surface of TOC surface and finally captured by the Ag NPs). Because the Schottky barrier effect at the Ag NPs/TOC interface and the Helmholtz capacitance effect at the Ag NPs/solution interface, which blocks carriers recombination and limits the release of captured electrons to solution. Consequently, holes accumulate on the surface of TOC side adjacent to Ag NPs/TOC boundaries, resulting in a significant oxidation reactions and disinfection action. It should mention that Ag has a well-known bactericidal capability by its own. It has been reported that Ag nanoclusters release Ag°, Ag^+ ions and Ag atoms can rapidly kill bacteria [104]. Ag^+ ions are strong electron donors can interact with thiol groups in cell proteins, causing inactivation of respiratory enzymes of bacteria [105]. To date, some mechanisms have been postulated for the bactericidal capability of Ag NPs: (i) Adhesion of Ag NPs to the surface of the bacteria changes the permeability of the membrane; [106] (ii) Ag NPs penetrate bacterial cells, resulting in DNA damage; (iii) dissolution of Ag NPs releases antimicrobial Ag^+ ions [105]. Thus, Ag itself can also display pronounced disinfection effect in the dark, which may also contribute the observed dark disinfection activity. The bactericidal effect caused by Ag is complex and requires specific analysis under specific systems and conditions.

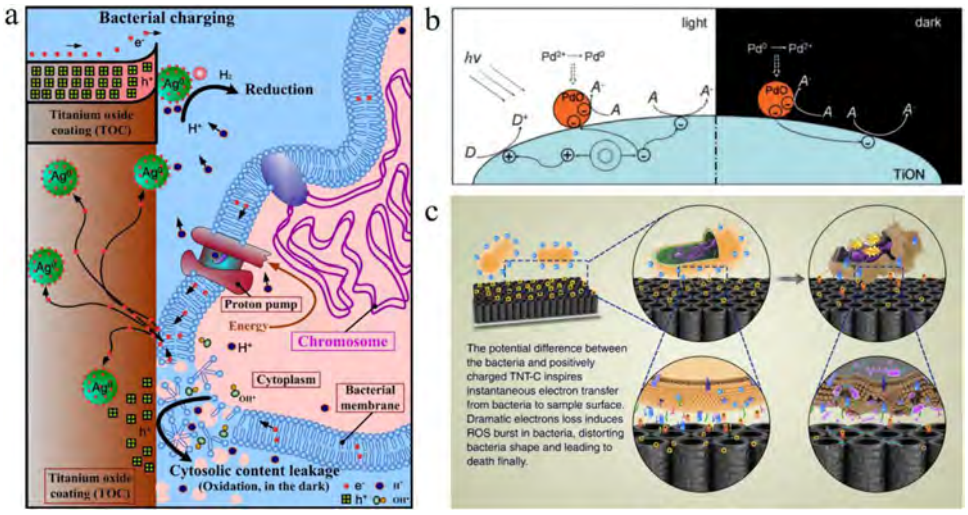

Fig. 12. (a) Illustration for extracellular electron transfer stimulated biocide action of Ag/TOC composites in the dark. That is, electrons are transferred from the bacterial membranes to the TOC surface, stored on the Ag NPs ("bacterial charging"), and induce valence-band hole (h^+) accumulation at the TOC side that explains cytosolic content leakage (Adapted with permission [63], Copyright 2012, Elsevier). (b) Schematic illustration of the process of photoelectrons flowing to PdO NPS on TiON matrix under visible light illumination and the process of discharging of PdO NPs when the visible light is switched off (Adapted with permission [95], Copyright 2010, Royal Society of Chemistry). (c) Diagram showing antibacterial mechanism. Proposed antibacterial process on DC + charged TNT-C based on the experimental results (Adapted with permission [110], Copyright 2018, Nature publishing group).

In addition to Ag NPs, Au NPs coupled with Cu_2O nanocrystals (Au@Cu_2O core@shell nanocrystals) has been synthesized by Lin et al. and use as the dual-functional catalyst that can continuously operate under illumination and darkness conditions for efficient E. coli inactivation [107]. They concluded that the bactericidal mechanism can be ascribed to the peroxidase mimics of the Au core and Fenton reactivity of the Cu_2O shell. Additionally, nanocomposite that composed of TiON/PdO was studied for the photocatalytic disinfection of E.coli under dark [95]. It was observed that PdO was the origin for the observed electron storage and dark anti-bacterial properties of the nanocomposite. Under light irradiation, the TiON can be excited to produce electron-hole pairs. The photogenerated electrons can transfer from TiON to PdO NPs and are partly captured by PdO NPs. These captured electrons may transfer back into the TiON or react with O_2/H_2O to generated radicals. The catalytic ability could be maintained even in the dark, as long as the electrons are released continuously, hence creating a catalytic memory effect (Fig. 12b). A similar mechanism was also reported for the antibacterial activity in the TiO_2/Cu_2O system towards *E.coli*, [108] SnO_2 NPs decorated Cu_2O nanocubes towards *Staphylococcus aureus* (*S. aureus*), [109] titanium oxide system [43] towards E. faecalis and E. coli under dark conditions.

Recently study suggested an external electrical current is applied to capacitive TiO_2 nanotubes doped with carbon (TNT-C), which can continue to kill bacteria after the positive direct current (DC+) power has been turned off. [110] The remarkable disinfection ability were due to the inherently excellent capacitance and discharging capacity. The stress in the bacteria was generated via interface electron transfer, which improved the production of intracellular ROS and deforms the morphology of bacteria, thereby leading to bacteria death (Fig. 12c). This mechanism is actually similar to the above-mentioned TiON/PdO mechanism, which both are based on the principle of carrier storage and release. The only difference is that the former is charged by the external electrical current while the latter is charged by the light radiation. The origin of the observed anti-bacterial activity of the two systems were both due to the generation of ROS which destroyed the structure of bacterial cell.

4.4. Hydrogen generation

$^{NCN}CN_x$ was demonstrated as a promising material for the generation of hydrogen in the dark [19,45,46]. In nature, photosynthesis in plants is the typical biological process for efficient energy conversion and utilization. Photosystems I and II separate the photo-generated carriers efficiently via the electron-transport chain, which divide the overall reaction into two halves, thereby inhibiting carrier recombination and back reaction. Calvin–Benson cycle is a "dark" process that utilizes the energy of storage electrons such as ATP to produce carbohydrates. Inspirited by this mechanism, V. Lotsch group reported an photocatalytic system that employs $^{NCN}CN_x$ as the catalyst, which can decouple the light and dark reactions to enable the hydrogen generation under dark [19]. They concluded this mechanism was due to the formation of long-lived radicals in cyanamide-functionalized polymeric network of heptazine units, which can release its captured electrons in the dark to generate hydrogen. As shown in Fig. 13(a, c), first involves production of the long-lived radical by pre-irradiating $^{NCN}CN_x$ suspension in the presence of electron donors. After illuminating, the reaction was put in the dark environment and then hydrogen is evolved with the addition of Pt colloid. The amount of hydrogen generated within 2 h usually reached maximizes after stop of illumination and the color of $^{NCN}CN_x$ reverse back to yellow (Fig. 13b). Fig. 13d showed that H_2 production in dark can be performed nearly12 h after illumination stopped, thereby demonstrating the reaction time of these long-lived radicals exceed the nighttime duration. A similar phenomenon was also appeared when Pt colloid was replaced with a NiP solution (Fig. 13e) [45].

4.5. Other applications

As mentioned, the classical application of electron storage system was the anticorrosion applications. It was reported that the corrosion property of TiO_2 coated type-304 stainless steel was suppressed under UV irradiation, however, as to protect the material even under dark [21]. Apart from removal of heavy metal ion, degradation pollutants, disinfection and hydrogen generation, how can we use stored electrons? Our group developed a method,

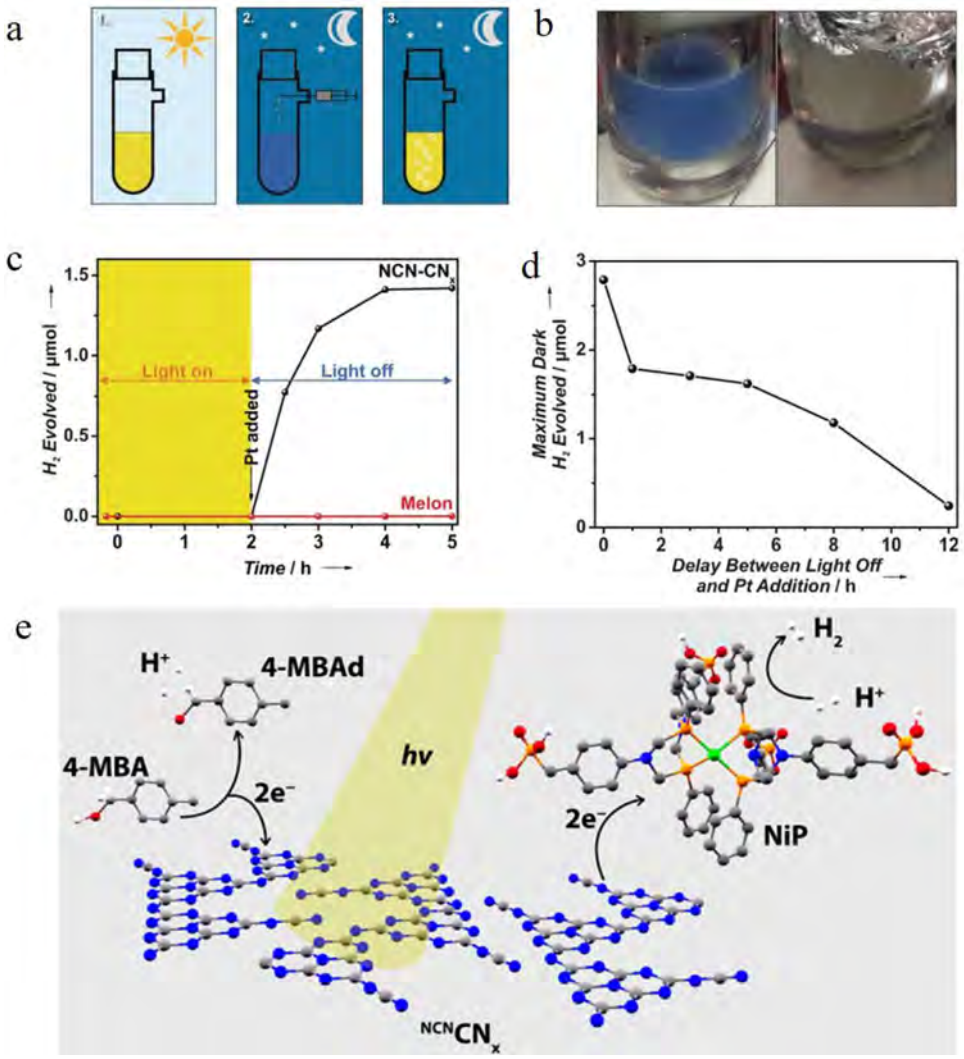

Fig. 13. (a) Schematic summary of the dark hydrogen evolution process: 1. Irradiation of the NCN-CN_x suspension to form the blue radical state; 2. Addition of a solution of hydrogen evolution cocatalyst under oxygen-free transfer in the dark, and 3. Evolution of hydrogen with the concomitant reversal of suspension color. (b) Photographs of the "blue radical" (left) and its color reversal subsequent to dark hydrogen evolution (right). (c) Plot illustrating the process of dark hydrogen evolution as a function of time, in which the region highlighted in yellow corresponds to the period of irradiation. (d) Maximum dark hydrogen evolved as a function of the time between switching off the light and injection of the Pt colloid (Adapted with permission [19], Copyright 2017, Wiley). (e) Schematic representation of a closed redox system for simultaneous proton reduction and alcohol oxidation in aqueous solution (Adapted with permission [45], Copyright 2016, American Chemical Society).

named "dark deposition" (DD) that Ag NPs can be deposited on the surface of TiO_2 in the dark [31]. Compared with traditional photo-deposition (PD), DD can inhibit the growth of Ag NPs. Generally speaking, smaller-sized Ag NPs have higher electron storage capacity over a range of sizes [62]. Therefore, Ag NPs in TiO_2@Ag prepared by DD (TiO_2@Ag-DD) have has maximum electron capacity (1 μmol/mg), higher than TiO_2 (0.11 μmol/mg) and TiO_2@Ag prepared by PD (TiO_2@Ag-PD) (0.35 μmol/mg). Mechanism and process of DD and PD was showed in Fig. 14(a, b). In absence of O_2, photogenerated electron on TiO_2 can be captured at the Ti^{3+} site. After turning off the light and adding $AgNO_3$, the captured electrons can be released and in situ reduce Ag^+ to metallic Ag NPs (Fig. 14a). Since the captured electrons are deterministic and no further electrons are generated, Ag NPs will uniformly formed on the surface of TiO_2 and will not grow further. Inversely, a mass of electrons are generated sustainability during the PD process. Once small Ag particles are formed, photogenerated electrons will rapidly transfer into Ag NPs, resulting in NPs growth because of the co-catalytic effect of metal NPs (Fig. 14b) [111]. Moreover, the enhanced "dark catalytic" activity was confirmed by various degradation experiments and mechanism was proposed in Fig. 14c. During the photocatalysis period, extra photogenerated electrons would be accumulated on Ag NPs due to its capacitive nature (charging). Then, the captured electrons can be released and react with appropriate electron acceptors such as O_2, H_2O_2, $S_2O_8^{2-}$, and BrO_3- to generate active radicals in the dark (discharging). TiO_2@Ag-DD as an all-day-active catalyst for the degradation of MO-MB mixture in natural sunlight was performed. Firstly, the degradation of the MO-MB mixture was carried out at daytime (afternoon, 04:30 p.m. local time). Subsequently, the degradation of residual MO-MB mixture was proceed with the addition of $S_2O_8^{2-}$ at nighttime (06:30 p.m. local time) (Fig. 14d). As shown in Fig. 14e, around 55 and 65% of MB and MO were degraded during daytime, respectively. Interestingly, the residual concentration of MO and MB further decreased at night due to the "dark catalytic" effect of as-prepared catalyst. This experiment displayed that the combination of photocatalysis and "dark catalytic" may offer a promising strategy for the continuous environmental purification in whole day.

In a sum, recent studies on the application of RTCPS are summarized in Table 1. It is well known that the photocatalysis is

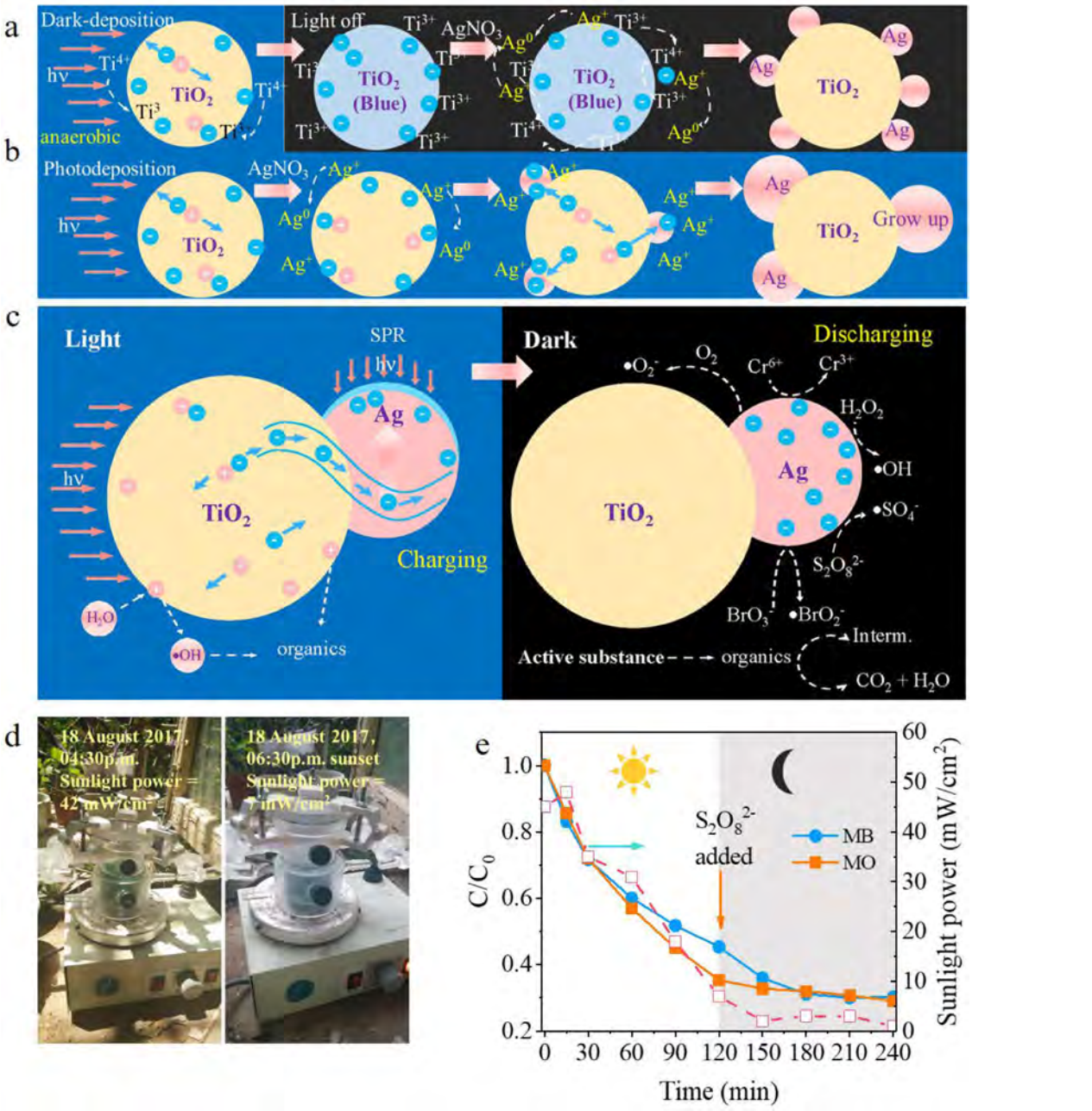

Fig. 14. Mechanism and Process of (a) DD and (b) PD. (c) Dark catalytic reaction mechanism. (d) Image of the MO-MB mixture solution degradation in the outdoor environment. (e) Removal of the MO-MB mixture solution in the outdoor environment. (Adapted with permission [31], Copyright 2018, American Chemical Society).

widely used for environmental purification and energy conversion applications. However, photocatalysis has other interesting applications, including (i) agricultural applications; [112] (ii) biodiesel productions; [113] (iii) medicinal applications (e.g., bio-implants [114,115] and cancer treatments [116,117]); and (iv) atmospheric sciences [118]. These potential applications should be combined with RTCPS to produce a more widespread applications.

4.6. Limitation in practical application

Although many potential applications in RTCPS including the removal of heavy metal ions, degradation of pollutant, disinfection and hydrogen generation have been reported, the present studies were in its infancy and the practice application might be impeded by many problems such as low reaction activity and short dark reaction time. The dark reduction of Cr^{6+} in Ag/TiO_2 system was only performed 300 min [29]. MB degradation by preirradiation Se NRs in the dark only can maintain 20 min and the degradation activity was very limited [65]. Although H_2 production in pre-irradiating $^{NCN}CN_x$ suspension can be performed nearly 12 h after illumination stopped, the yield of H_2 is not optimistic [19]. For electron storage system, the key issue is to increase the electronic storage capacity and to properly control the electron release rate. For fluorescence-assisted system, how to enhance the absorption of light by long afterglow phosphors is the key to improve dark reaction activity. In a sum, more effort is required to design more efficient RTCPS with high reaction activity and long reaction time for future practice applications.

Table 1
A summary of the mechanism and application of different round-the-clock photocatalytic systems.

Catalytic system	Mechanism	Applications	Reference
TiO_2-WO_3	Electron storage	Anticorrosion	[21]
TiO_2-WO_3	Electron storage	Reduction of Cr^{6+}, Hg^{2+}, and Ag^+	[28]
TiO_2/Ag	Electron storage	Reduction of Cr^{6+}	[29]
TiO_2-$Ni(OH)_2$	Hole storage	Degradation of alcohols, aldehydes, phenol, etc.	[69]
TiO_2-$Ni(OH)_2$	Hole storage	Oxidation of methanol and formaldehyde	[70]
$TiO_2/SiO_2/MnO_x$	Hole storage	Oxidation of multicarbon compounds	[75]
TiON[a]/PdO	Electron storage	Degradation of MB[b]	[20]
Se nanorod	Electron storage	Degradation of MB	[65]
Pt–$HCa_2Nb_3O_{10}$	Electron storage	Degradation of MO[c] and methanol	[32]
WO_3/TiO_2	Electron storage	Degradation of MO	[34]
C_3N_4/CNTs[d]/graphene	Electron storage	Degradation of phenol	[38]
TiO_2-Au@Cu_7S_4	Peroxidase mimic	Degradation of MO	[22]
g-C_3N_4/ $Sr_2MgSi_2O_7$: (Eu, Dy)	Fluorescence assist	Degradation of MO and RhB[e]	[17]
Cu_2O/TiO_2	Fluorescence assist	Degradation of RhB and BPA[f]	[87]
$Ag_3PO_4/Sr_4Al_{14}O_{25}$: (Eu, Dy)	Fluorescence assist	Degradation of RhB	[88]
$CaAl_2O_4$:(Eu, Nd)/$TiO_{2-x}N_y$[g]	Fluorescence assist	Degradation of NO	[90]
$CaAl_2O_4$:(Eu, Nd)/$TiO_{2-x}N_y$	Fluorescence assist	Degradation of acetaldehyde	[23]
TiO_2–WO_3	Electron storage	Disinfection (*E. coli*[h])	[39]
Ag NPs/TiO_2 coatings	Electron storage	Disinfection (*S. aureus*[i] and *E. coli*)	[63]
TiON/PdO	Electron storage	Disinfection (*E. coli*)	[95]
TiO_2/Cu_2O	Electron storage	Disinfection (*E. coli*)	[108]
SnO_2/Cu_2O	Electron storage	Disinfection (*S. aureus*)	[109]
TiO_2 nanosheets	Electron storage	Disinfection (*E. faecalis*[j] and *E. coli*)	[43]
TNT-C[k]	Hole storage	Disinfection (*S. aureus* and *E. coli*)	[110]
$^{NCN}CN_x$[l]	Electron storage	Hydrogen generation	[19]
$^{NCN}CN_x$	Electron storage	Hydrogen generation	[45]
CCN[m]	Electron storage	Hydrogen generation	[46]
TiO_2@Ag	Electron storage	Deposition method	[31]

[a] TiON: nitrogen-doped TiO_2.
[b] MB: methylene blue.
[c] MO: methyl orange.
[d] CNTs: carbon nanotube.
[e] RhB: rhodamine.
[f] BPA: bisphenol A.
[g] $TiO_{2-x}N_y$: nitrogen-doped TiO_2.
[h] *E. coli*: *Escherichia coli*.
[i] *S. aureus*: *Staphylococcus aureus*.
[j] *E. faecalis*: *Escherichia faecalis*.
[k] TNT-C: carbon-doped TiO_2 nanotubes.
[l] $NCNCN_x$: cyanamide-functionalized heptazine-based polymer.
[m] CNN: cyano-groups modified g-C_3N_4.

5. Conclusion and outlook

At present, there are four mechanisms for RTCP, namely, electron storage mechanism, hole storage mechanism, peroxidase mimic mechanism and fluorescence-assisted mechanism. Among them, most RTCPS are based on electron storage mechanisms. This system is generally composes of two kinds of materials, a SC and an ESS. Under irradiation, SC as the photocatalyst provided photogenerated electrons while ESS as electron sink trap the electrons from SC. When light is removed, ESS can release the trapped electrons to appropriate electron acceptors such as O_2 and H^+, etc. "Dark catalysis" activity arise from the reaction of released electron and electron acceptors, which have been widely used in the field of environment and energy, especially, disinfection and pollutant removal. The "dark catalysis" activity is related to the electron storage capacity. In TiO_2-WO_3 system, amount of charges stored is demonstrated to be dependent on the M^+ ionic radii. The electron storage capacity ascends with increasing ionic radii, which can be elucidated by the ability of larger ions to remain in the structure for a longer period of time. In TiO_2/Ag system, The electron storage capacity are mainly dependent on the size of Ag NPs. Smaller-sized Ag NPs were demonstrated to have higher electron capacity. High valence metal oxide such as WO_3 can store electrons mainly due to the abundant valence change of high valence metal ion (e.g., W^{+6}, W^{+5}, etc.). Intercalation of ions stabilizes materials to maintain electrical neutrality. While the electron storage ability of Ag NPs stem from its capacitive nature, which can trap electrons and impedes the charge transfer out of its surface.

It should be pointed out that recent RTCPS are mostly discovered in TiO_2, WO_3, Ag and C_3N_4 based material system, whereas the study of other systems are still limited. Developing new materials system may provide more opportunities for future studies. Although many advance characterization techniques have been developed to study the charge and discharge process of trapped electrons, more intuitive characterization methods are still very limited. It is also of great significance to develop some methods to precisely and quantitatively estimate the electron storage capacity. Note that present study is still at the infant stage and there are still many problems in practical applications such as low reactivity of electrons and short reactive time during dark period. Moreover, the application range of RTCP is also very limited. However, it should point out that by designing new photocatalytic reactor and coupled with other technology can improve the practical utilities of RTCPS. For example, Li et. al. developed a new RTCPS involved a photocatalytic reactor equipped with solar batteries [119]. The Bi_2O_3/TiO_2 photocatalyst started photocatalytic degradation of organonitrogen compounds under sunlight. Meanwhile, solar batteries convert sunlight into stored electrical energy to started UV lamps at night, leading to RTCP degradation of pollutants. Additionally, inorganic nitrogen species resulting from organonitrogen compounds degradation can be absorbed by the plant as a fertilizer, which further reduce the secondary pollution. It is also of great significance to study the combination of RTCPS

and advanced oxidation technology to further advance its practical application. Further investigations of this system may find more appropriate applications.

Acknowledgments

This work was supported by the National Natural Science Foundation of China (51872089, 51478171 and 51672077) and Hunan Provincial Natural Science Foundation of China (2017JJ2026).

References

[1] P. Zhou, J. Yu, M. Jaroniec, All-solid-state Z-scheme photocatalytic systems, Adv. Mater. 26 (2014) 4920–4935.
[2] N.S. Lewis, Toward cost-effective solar energy use, Science 315 (2007) 798–801.
[3] T. Hisatomi, J. Kubota, K. Domen, Recent advances in semiconductors for photocatalytic and photoelectrochemical water splitting, Chem. Soc. Rev. 43 (2014) 7520–7535.
[4] Y. Moriya, T. Takata, K. Domen, Recent progress in the development of (oxy) nitride photocatalysts for water splitting under visible-light irradiation, Coord. Chem. Rev. 257 (2013) 1957–1969.
[5] A. Fujishima, K. Honda, Electrochemical photolysis of water at a semiconductor electrode, Nature 238 (1972) 37.
[6] S. Bai, J. Jiang, Q. Zhang, Y. Xiong, Steering charge kinetics in photocatalysis: intersection of materials syntheses, characterization techniques and theoretical simulations, Chem. Soc. Rev. 44 (2015) 2893–2939.
[7] A.L. Linsebigler, G. Lu, J.T. Yates Jr, Photocatalysis on TiO_2 surfaces: principles, mechanisms, and selected results, Chem. Rev. 95 (1995) 735–758.
[8] J. Schneider, M. Matsuoka, M. Takeuchi, J. Zhang, Y. Horiuchi, M. Anpo, D.W. Bahnemann, Understanding TiO_2 photocatalysis: mechanisms and materials, Chem. Rev. 114 (2014) 9919–9986.
[9] C. Liu, L. Wang, Y. Tang, S. Luo, Y. Liu, S. Zhang, Y. Zeng, Y. Xu, Vertical single or few-layer MoS_2 nanosheets rooting into TiO_2 nanofibers for highly efficient photocatalytic hydrogen evolution, Appl. Catal. B 164 (2015) 1–9.
[10] L. Wang, X. Duan, G. Wang, C. Liu, S. Luo, S. Zhang, Y. Zeng, Y. Xu, Y. Liu, X. Duan, Omnidirectional enhancement of photocatalytic hydrogen evolution over hierarchical "cauline leaf" nanoarchitectures, Appl. Catal. B 186 (2016) 88–96.
[11] L. Wang, X. Liu, J. Luo, X. Duan, J. Crittenden, C. Liu, S. Zhang, Y. Pei, Y. Zeng, X. Duan, Self-optimization of the active site of molybdenum disulfide by an irreversible phase transition during photocatalytic hydrogen evolution, Angew. Chem. 129 (2017) 7718–7722.
[12] S. Zhang, L. Wang, C. Liu, J. Luo, J. Crittenden, X. Liu, T. Cai, J. Yuan, Y. Pei, Y. Liu, Photocatalytic wastewater purification with simultaneous hydrogen production using MoS_2 QD-decorated hierarchical assembly of $ZnIn_2S_4$ on reduced graphene oxide photocatalyst, Water Res. 121 (2017) 11–19.
[13] S. Zhang, X. Liu, C. Liu, S. Luo, L. Wang, T. Cai, Y. Zeng, J. Yuan, W. Dong, Y. Pei, Y. Liu, MoS_2 quantum dot growth induced by S vacancies in a $ZnIn_2S_4$ monolayer: atomic-level heterostructure for photocatalytic hydrogen production, ACS Nano 12 (2018) 751–758.
[14] J. Wang, L. Tang, G. Zeng, Y. Deng, Y. Liu, L. Wang, Y. Zhou, Z. Guo, J. Wang, C. Zhang, Atomic scale g-C_3N_4/Bi_2WO_6 2D/2D heterojunction with enhanced photocatalytic degradation of ibuprofen under visible light irradiation, Appl. Catal. B 209 (2017) 285–294.
[15] T. Cai, Y. Liu, L. Wang, S. Zhang, Y. Zeng, J. Yuan, J. Ma, W. Dong, C. Liu, S. Luo, Silver phosphate-based Z-Scheme photocatalytic system with superior sunlight photocatalytic activities and anti-photocorrosion performance, Appl. Catal. B 208 (2017) 1–13.
[16] W. Dong, Y. Liu, G. Zeng, S. Zhang, T. Cai, J. Yuan, H. Chen, J. Gao, C. Liu, Regionalized and vectorial charges transferring of $Cd_{1-x}Zn_xS$ twin nanocrystal homojunctions for visible-light driven photocatalytic applications, J. Colloid Interface Sci. 518 (2018) 156–164.
[17] Q. Zhou, F. Peng, Y. Ni, J. Kou, C. Lu, Z. Xu, Long afterglow phosphor driven round-the-clock g-C_3N_4 photocatalyst, J. Photochem. Photobiol. A: Chem. 328 (2016) 182–188.
[18] M. Sakar, C.C. Nguyen, M.H. Vu, T.O. Do, Materials and mechanisms of photo-assisted chemical reactions under light and dark conditions: can day-night photocatalysis be achieved? ChemSusChem 11 (2018) 809–820.
[19] V.Wh. Lau, D. Klose, H. Kasap, F. Podjaski, M.C. Pignié, E. Reisner, G. Jeschke, B.V. Lotsch, Dark photocatalysis: storage of solar energy in carbon nitride for time-delayed hydrogen generation, Angew. Chem. Int. Ed. 56 (2017) 510–514.
[20] Q. Li, Y.W. Li, P. Wu, R. Xie, J.K. Shang, Palladium oxide nanoparticles on nitrogen-doped titanium oxide: accelerated photocatalytic disinfection and post-illumination catalytic "Memory", Adv. Mater. 20 (2008) 3717–3723.
[21] T. Tatsuma, S. Saitoh, Y. Ohko, A. Fujishima, TiO_2– WO_3 photoelectrochemical anticorrosion system with an energy storage ability, Chem. Mater. 13 (2001) 2838–2842.
[22] Y.-H. Chiu, Y.-J. Hsu, Au@Cu_7S_4 yolk@shell nanocrystal-decorated TiO_2 nanowires as an all-day-active photocatalyst for environmental purification, Nano Energy 31 (2017) 286–295.
[23] H. Li, S. Yin, Y. Wang, T. Sato, Persistent fluorescence-assisted $TiO_{2-x}N_y$-based photocatalyst for gaseous acetaldehyde degradation, Environ. Sci. Technol. 46 (2012) 7741–7745.
[24] H. Li, S. Yin, Y. Wang, T. Sato, Effect of phase structures of $TiO_{2-x}N_y$ on the photocatalytic activity of $CaAl_2O_4$:(Eu, Nd)-coupled $TiO_{2-x}N_y$, J. Catal. 286 (2012) 273–278.
[25] H. Li, S. Yin, Y. Wang, T. Sato, Blue fluorescence-assisted $SrTi_{1-x}Cr_yO_3$ for efficient persistent photocatalysis, RSC Adv. 2 (2012) 3234–3236.
[26] H. Li, S. Yin, Y. Wang, T. Sato, Efficient persistent photocatalytic decomposition of nitrogen monoxide over a fluorescence-assisted $CaAl_2O_4$:(Eu, Nd)/(Ta, N)-codoped TiO_2/Fe_2O_3, Appl. Catal. B 132–133 (2013) 487–492.
[27] F. Li, Z. Li, Y. Cai, M. Zhang, Y. Shen, W. Wang, Afterglow photocatalysis of Ag_3PO_4 through different afterglow coatings and photocatalysis mechanism, Mater. Lett. 208 (2017) 111–114.
[28] D. Zhao, C. Chen, C. Yu, W. Ma, J. Zhao, Photoinduced electron storage in WO_3/TiO_2 nanohybrid material in the presence of oxygen and postirradiated reduction of heavy metal ions, J Phys. Chem. C 113 (2009) 13160–13165.
[29] Y. Choi, M.S. Koo, A.D. Bokare, D.H. Kim, D.W. Bahnemann, W. Choi, Sequential process combination of photocatalytic oxidation and dark reduction for the removal of organic pollutants and Cr(VI) using Ag/TiO_2, Environ. Sci. Technol. 51 (2017) 3973–3981.
[30] S. Park, W. Kim, R. Selvaraj, Y. Kim, Spontaneous reduction of Cr(VI) using $InSnS_2$ under dark condition, Chem. Eng. J. 321 (2017) 97–104.
[31] T. Cai, Y. Liu, L. Wang, S. Zhang, J. Ma, W. Dong, Y. Zeng, J. Yuan, C. Liu, S. Luo, "Dark deposition" of Ag nanoparticles on TiO_2: improvement of electron storage capacity to boost "memory catalysis" activity, ACS Appl. Mater. Interfaces 10 (2018) 25350–25359.
[32] E. Dvininov, U.A. Joshi, J.R. Darwent, J.B. Claridge, Z. Xu, M.J. Rosseinsky, Room temperature oxidation of methyl orange and methanol over Pt-$HCa_2Nb_3O_{10}$ and Pt-WO_3 catalysts without light, Chem. Commun. (Camb.) 47 (2011) 881–883.
[33] D. Su, J. Wang, Y. Tang, C. Liu, L. Liu, X. Han, Constructing WO_3/TiO_2 composite structure towards sufficient use of solar energy, Chem. Commun. (Camb.) 47 (2011) 4231–4233.
[34] Y. Li, L. Chen, Y. Guo, X. Sun, Y. Wei, Preparation and characterization of WO_3/TiO_2 hollow microsphere composites with catalytic activity in dark, Chem. Eng. J. 181–182 (2012) 734–739.
[35] A. Molla, M. Sahu, S. Hussain, Under dark and visible light: fast degradation of methylene blue in the presence of Ag–In–Ni–S nanocomposites, J. Mater. Chem. A 3 (2015) 15616–15625.
[36] A. Molla, M. Sahu, S. Hussain, Synthesis of tunable band gap semiconductor nickel sulphide nanoparticles: rapid and round the clock degradation of organic dyes, Sci. Rep. 6 (2016) 26034.
[37] C.-C. Nguyen, N.-N. Vu, T.-O. Do, Efficient hollow double-shell photocatalysts for the degradation of organic pollutants under visible light and in darkness, J. Mater. Chem. A 4 (2016) 4413–4419.
[38] Q. Zhang, H. Wang, Z. Li, C. Geng, J. Leng, Metal-free photocatalyst with visible-light-driven post-illumination catalytic memory, ACS Appl. Mater. Interfaces 9 (2017) 21738–21746.
[39] T. Tatsuma, S. Takeda, S. Saitoh, Y. Ohko, A. Fujishima, Bactericidal effect of an energy storage TiO_2–WO_3 photocatalyst in dark, Electrochem. Commun. 5 (2003) 793–796.
[40] Y. Takahashi, P. Ngaotrakanwiwat, T. Tatsuma, Energy storage TiO_2–MoO_3 photocatalysts, Electrochim. Acta 49 (2004) 2025–2029.
[41] H. Lin, W. Deng, T. Zhou, S. Ning, J. Long, X. Wang, Iodine-modified nanocrystalline titania for photo-catalytic antibacterial application under visible light illumination, Appl. Catal. B 176–177 (2015) 36–43.
[42] L. Liu, W. Sun, W. Yang, Q. Li, J.K. Shang, Post-illumination activity of SnO_2 nanoparticle-decorated Cu_2O nanocubes by H_2O_2 production in dark from photocatalytic memory, Sci. Rep. 6 (2016) 20878.
[43] G. Wang, Z. Xing, X. Zeng, C. Feng, D.T. McCarthy, A. Deletic, X. Zhang, Ultrathin titanium oxide nanosheets film with memory bactericidal activity, Nanoscale 8 (2016) 18050–18056.
[44] J. Gupta, J. Mohapatra, D. Bahadur, Visible light driven mesoporous Ag-embedded ZnO nanocomposites: reactive oxygen species enhanced photocatalysis, bacterial inhibition and photodynamic therapy, Dalton Trans. 46 (2017) 685–696.
[45] H. Kasap, C.A. Caputo, B.C. Martindale, R. Godin, V.W. Lau, B.V. Lotsch, J.R. Durrant, E. Reisner, Solar-driven reduction of aqueous protons coupled to selective alcohol oxidation with a carbon nitride-molecular Ni catalyst system, J. Am. Chem. Soc. 138 (2016) 9183–9192.
[46] Z. Zeng, X. Quan, H. Yu, S. Chen, Y. Zhang, H. Zhao, S. Zhang, Carbon nitride with electron storage property: enhanced exciton dissociation for high-efficient photocatalysis, Appl. Catal. B 236 (2018) 99–106.
[47] K. Maeda, Z-scheme water splitting using two different semiconductor photocatalysts, ACS Catal. 3 (2013) 1486–1503.
[48] M.A. Fox, M.T. Dulay, Heterogeneous photocatalysis, Chem. Rev. 93 (1993) 341–357.
[49] G. Knör, Recent progress in homogeneous multielectron transfer photocatalysis and artificial photosynthetic solar energy conversion, Coord. Chem. Rev. 304 (2015) 102–108.
[50] X. Jin, L. Ye, H. Xie, G. Chen, Bismuth-rich bismuth oxyhalides for environmental and energy photocatalysis, Coord. Chem. Rev. 349 (2017) 84–101.

[51] Y. Fang, Y. Ma, M. Zheng, P. Yang, A.M. Asiri, X. Wang, Metal–organic frameworks for solar energy conversion by photoredox catalysis, Coord. Chem. Rev. (2017) 83–115.
[52] P. Ngaotrakanwiwat, T. Tatsuma, S. Saitoh, Y. Ohko, A. Fujishima, Charge–discharge behavior of TiO_2–WO_3 photocatalysis systems with energy storage ability, Phys. Chem. Chem. Phys. 5 (2003) 3234–3237.
[53] H. Park, A. Bak, T.H. Jeon, S. Kim, W. Choi, Photo-chargeable and dischargeable TiO_2 and WO_3 heterojunction electrodes, Appl. Catal. B 115–116 (2012) 74–80.
[54] P. Ngaotrakanwiwat, T. Tatsuma, Optimization of energy storage TiO_2–WO_3 photocatalysts and further modification with phosphotungstic acid, J. Electroanal. Chem. 573 (2004) 263–269.
[55] C. Ng, Y.H. Ng, A. Iwase, R. Amal, Visible light-induced charge storage, on-demand release and self-photorechargeability of WO_3 film, Phys. Chem. Chem. Phys. 13 (2011) 13421–13426.
[56] Y. Takahashi, T. Tatsuma, Visible light-induced photocatalysts with reductive energy storage abilities, Electrochem. Commun. 10 (2008) 1404–1407.
[57] S. Kim, Y. Park, W. Kim, H. Park, Harnessing and storing visible light using a heterojunction of WO_3 and CdS for sunlight-free catalysis, Photochem. Photobiol. Sci. 15 (2016) 1006–1011.
[58] F. Feng, W. Yang, S. Gao, C. Sun, Q. Li, Postillumination activity in a single-phase photocatalyst of Mo-doped TiO_2 nanotube array from its photocatalytic "memory", ACS Sustain. Chem. Eng. 6 (2018) 6166–6174.
[59] A. Kongkanand, P.V. Kamat, Electron storage in single wall carbon nanotubes. Fermi level equilibration in semiconductor–SWCNT suspensions, ACS Nano 1 (2007) 13–21.
[60] Z. Yang, L. Li, Y. Luo, R. He, L. Qiu, H. Lin, H. Peng, An integrated device for both photoelectric conversion and energy storage based on free-standing and aligned carbon nanotube film, J. Mater. Chem. A 1 (2013) 954–958.
[61] A. Wood, M. Giersig, P. Mulvaney, Fermi level equilibration in quantum dot–metal nanojunctions, J. Phys. Chem. B 105 (2001) 8810–8815.
[62] A. Takai, P.V. Kamat, Capture, store, and discharge. Shuttling photogenerated electrons across TiO_2–silver interface, ACS Nano 5 (2011) 7369–7376.
[63] H. Cao, Y. Qiao, X. Liu, T. Lu, T. Cui, F. Meng, P.K. Chu, Electron storage mediated dark antibacterial action of bound silver nanoparticles: smaller is not always better, Acta Biomater. 9 (2013) 5100–5110.
[64] M.D. Scanlon, P. Peljo, M.A. Mendez, E. Smirnov, H.H. Girault, Charging and discharging at the nanoscale: fermi level equilibration of metallic nanoparticles, Chem. Sci. 6 (2015) 2705–2720.
[65] Y.-D. Chiou, Y.-J. Hsu, Room-temperature synthesis of single-crystalline Se nanorods with remarkable photocatalytic properties, Appl. Catal. B 105 (2011) 211–219.
[66] F. Dong, T. Xiong, Y. Sun, Z. Zhao, Y. Zhou, X. Feng, Z. Wu, A semimetal bismuth element as a direct plasmonic photocatalyst, Chem. Commun. (Camb) 50 (2014) 10386–10389.
[67] J. Yasomanee, J. Bandara, Multi-electron storage of photoenergy using Cu_2O–TiO_2 thin film photocatalyst, Sol. Energy Mater. Sol. Cells 92 (2008) 348–352.
[68] C.-T. Wang, H.-H. Huang, Photo-chargeable titanium/vanadium oxide composites, J. Non-Cryst. Solids 354 (2008) 3336–3342.
[69] Y. Takahashi, T. Tatsuma, Oxidative Energy Storage Ability of a TiO_2–$Ni(OH)_2$ Bilayer Photocatalyst, Langmuir 21 (2005) 12357–12361.
[70] F. Yang, Y. Takahashi, N. Sakai, T. Tatsuma, Oxidation of methanol and formaldehyde to CO_2 by a photocatalyst with an energy storage ability, Phys. Chem. Chem. Phys. 12 (2010) 5166–5170.
[71] F. Yang, Y. Takahashi, N. Sakai, T. Tatsuma, Visible light driven photocatalysts with oxidative energy storage abilities, J. Mater. Chem. 21 (2011) 2288–2293.
[72] L. Zhang, L. Xu, J. Wang, J. Cai, J. Xu, H. Zhou, Y. Zhong, D. Chen, J. Zhang, C.-n. Cao, Enhanced energy storage of a UV-irradiated three-dimensional nanostructured TiO_2–$Ni(OH)_2$ composite film and its electrochemical discharge in the dark, J. Electroanal. Chem. 683 (2012) 55–61.
[73] H. Huang, L. Jiang, W.K. Zhang, Y.P. Gan, X.Y. Tao, H.F. Chen, Photoelectrochromic properties and energy storage of $TiO_{2-x}N_x$/NiO bilayer thin films, Sol. Energy Mater. Sol. Cells 94 (2010) 355–359.
[74] S. Buama, A. Junsukhon, P. Ngaotrakanwiwat, P. Rangsunvigit, Validation of energy storage of TiO_2 NiO/TiO_2 film by electrochemical process and photocatalytic activity, Chem. Eng. J. 309 (2017) 866–872.
[75] Y. Kuroiwa, S. Park, N. Sakai, T. Tatsuma, Oxidation of multicarbon compounds to CO_2 by photocatalysts with energy storage abilities, Phys. Chem. Chem. Phys. 18 (2016) 31441–31445.
[76] M. Ma, Y. Zhang, N. Gu, Peroxidase-like catalytic activity of cubic Pt nanocrystals, Colloid Surf. A 373 (2011) 6–10.
[77] W. Shi, Q. Wang, Y. Long, Z. Cheng, S. Chen, H. Zheng, Y. Huang, Carbon nanodots as peroxidase mimetics and their applications to glucose detection, Chem. Commun. (Camb.) 47 (2011) 6695–6697.
[78] Y. Song, K. Qu, C. Zhao, J. Ren, X. Qu, Graphene oxide: intrinsic peroxidase catalytic activity and its application to glucose detection, Adv. Mater. 22 (2010) 2206–2210.
[79] R. Cui, Z. Han, J.J. Zhu, Helical carbon nanotubes: intrinsic peroxidase catalytic activity and its application for biocatalysis and biosensing, Chemistry 17 (2011) 9377–9384.
[80] J. Yin, H. Cao, Y. Lu, Self-assembly into magnetic Co_3O_4 complex nanostructures as peroxidase, J. Mater. Chem. 22 (2012) 527–534.
[81] L. Chen, B. Sun, X. Wang, F. Qiao, S. Ai, 2D ultrathin nanosheets of Co–Al layered double hydroxides prepared in l-asparagine solution: enhanced peroxidase-like activity and colorimetric detection of glucose, J. Mater. Chem. B 1 (2013) 2268–2274.
[82] Y. Zhang, C. Xu, B. Li, Y. Li, In situ growth of positively-charged gold nanoparticles on single-walled carbon nanotubes as a highly active peroxidase mimetic and its application in biosensing, Biosens. Bioelectron. 43 (2013) 205–210.
[83] Z. Gao, M. Xu, L. Hou, G. Chen, D. Tang, Irregular-shaped platinum nanoparticles as peroxidase mimics for highly efficient colorimetric immunoassay, Anal. Chim. Acta. 776 (2013) 79–86.
[84] L. Su, J. Feng, X. Zhou, C. Ren, H. Li, X. Chen, Colorimetric detection of urine glucose based $ZnFe_2O_4$ magnetic nanoparticles, Anal. Chem. 84 (2012) 5753–5758.
[85] X. Chen, X. Tian, B. Su, Z. Huang, X. Chen, M. Oyama, Au nanoparticles on citrate-functionalized graphene nanosheets with a high peroxidase-like performance, Dalton Trans. 43 (2014) 7449–7454.
[86] Z. Zhang, A. Berg, H. Levanon, R.W. Fessenden, D. Meisel, On the interactions of free radicals with gold nanoparticles, J. Am. Chem. Soc. 125 (2003) 7959–7963.
[87] Y. Lu, X. Zhang, Y. Chu, H. Yu, M. Huo, J. Qu, J.C. Crittenden, H. Huo, X. Yuan, Cu_2O nanocrystals/TiO_2 microspheres film on a rotating disk containing long-afterglow phosphor for enhanced round-the-clock photocatalysis, Appl. Catal. B 224 (2018) 239–248.
[88] H. Li, S. Yin, Y. Wang, T. Sekino, S.W. Lee, T. Sato, Green phosphorescence-assisted degradation of rhodamine Bdyes by Ag_3PO_4, J. Mater. Chem. A 1 (2013) 1123–1126.
[89] H. Yin, X. Chen, R. Hou, H. Zhu, S. Li, Y. Huo, H. Li, Ag/BiOBr film in a rotating-disk reactor containing long-afterglow phosphor for round-the-clock photocatalysis, ACS Appl. Mater. Interfaces 7 (2015) 20076–20082.
[90] H. Li, S. Yin, T. Sato, Novel luminescent photocatalytic $deNO_x$ activity of $CaAl_2O_4$:(Eu,Nd)/$TiO_{2-x}N_y$ composite, Appl. Catal. B 106 (2011) 586–591.
[91] D. Liu, W. Zi, S.D. Sajjad, C. Hsu, Y. Shen, M. Wei, F. Liu, Reversible electron storage in an all-vanadium photoelectrochemical storage cell: synergy between vanadium redox and hybrid photocatalyst, ACS Catal. 5 (2015) 2632–2639.
[92] L. Zhang, W. Wang, S. Sun, D. Jiang, Near-infrared light photocatalysis with metallic/semiconducting H_xWO_3/WO_3 nanoheterostructure in situ formed in mesoporous template, Appl. Catal. B 168–169 (2015) 9–13.
[93] O. Schirmer, V. Wittwer, G. Baur, G. Brandt, Dependence of WO_3 electrochromic absorption on crystallinity, J. Electrochem. Soc. 124 (1977) 749–753.
[94] A. Hjelm, C.G. Granqvist, J.M. Wills, Electronic structure and optical properties of WO_3, $LiWO_3$, $NaWO_3$, and HWO_3, Phys. Rev. B 54 (1996) 2436.
[95] Q. Li, Y.W. Li, Z. Liu, R. Xie, J.K. Shang, Memory antibacterial effect from photoelectron transfer between nanoparticles and visible light photocatalyst, J. Mater. Chem. 20 (2010) 1068–1072.
[96] R. Chen, S. Pang, H. An, J. Zhu, S. Ye, Y. Gao, F. Fan, C. Li, Charge separation via asymmetric illumination in photocatalytic Cu_2O particles, Nat. Energy 3 (2018) 655–663.
[97] M. Jakob, H. Levanon, P.V. Kamat, Charge distribution between UV-irradiated TiO_2 and gold nanoparticles: determination of shift in the Fermi level, Nano Lett. 3 (2003) 353–358.
[98] I.V. Lightcap, T.H. Kosel, P.V. Kamat, Anchoring semiconductor and metal nanoparticles on a two-dimensional catalyst mat. Storing and shuttling electrons with reduced graphene oxide, Nano Lett. 10 (2010) 577–583.
[99] Y. Ying, Y. Liu, X. Wang, Y. Mao, W. Cao, P. Hu, X. Peng, Two-dimensional titanium carbide for efficiently reductive removal of highly toxic chromium(VI) from water, ACS Appl. Mater. Interfaces 7 (2015) 1795–1803.
[100] I. Robel, B.A. Bunker, P.V. Kamat, Single-walled carbon nanotube-CdS Nanocomposites as light-harvesting assemblies: photoinduced charge-transfer interactions, Adv. Mater. 17 (2005) 2458–2463.
[101] M. Zhi, C. Xiang, J. Li, M. Li, N. Wu, Nanostructured carbon–metal oxide composite electrodes for supercapacitors: a review, Nanoscale 5 (2013) 72–88.
[102] K. Sunada, Y. Kikuchi, K. Hashimoto, A. Fujishima, Bactericidal and detoxification effects of TiO_2 thin film photocatalysts, Environ. Sci. Technol. 32 (1998) 726–728.
[103] P. Wu, J.A. Imlay, J.K. Shang, Mechanism of *Escherichia coli* inactivation on palladium-modified nitrogen-doped titanium dioxide, Biomaterials 31 (2010) 7526–7533.
[104] A. Kubacka, M. Ferrer, A. Martínez-Arias, M. Fernández-García, Ag promotion of TiO_2-anatase disinfection capability: study of *Escherichia coli* inactivation, Appl. Catal. B 84 (2008) 87–93.
[105] Q. Li, S. Mahendra, D.Y. Lyon, L. Brunet, M.V. Liga, D. Li, P.J. Alvarez, Antimicrobial nanomaterials for water disinfection and microbial control: potential applications and implications, Water Res. 42 (2008) 4591–4602.
[106] I. Sondi, B. Salopek-Sondi, Silver nanoparticles as antimicrobial agent: a case study on *E. coli* as a model for Gram-negative bacteria, J. Colloid Interface Sci. 275 (2004) 177–182.
[107] M.-Y. Kuo, C.-F. Hsiao, Y.-H. Chiu, T.-H. Lai, M.-J. Fang, J.-Y. Wu, J.-W. Chen, C.-L. Wu, K.-H. Wei, H.-C. Lin, Y.-J. Hsu, Au@Cu_2O core@shell nanocrystals as dual-functional catalysts for sustainable environmental applications, Appl. Catal. B 242 (2019) 499–506.
[108] L. Liu, W. Yang, Q. Li, S. Gao, J.K. Shang, Synthesis of Cu_2O nanospheres decorated with TiO_2 nanoislands, their enhanced photoactivity and stability

under visible light illumination, and their post-illumination catalytic memory, ACS Appl. Mater. Interfaces 6 (2014) 5629–5639.
[109] L. Liu, W. Sun, W. Yang, Q. Li, J.K. Shang, Post-illumination activity of SnO_2 nanoparticle-decorated Cu_2O nanocubes by H_2O_2 production in dark from photocatalytic "memory", Sci. Rep. 6 (2016) 20878.
[110] G. Wang, H. Feng, L. Hu, W. Jin, Q. Hao, A. Gao, X. Peng, W. Li, K.Y. Wong, H. Wang, Z. Li, P.K. Chu, An antibacterial platform based on capacitive carbon-doped TiO_2 nanotubes after direct or alternating current charging, Nat. Commun. 9 (2018) 2055.
[111] K. Wenderich, G. Mul, Methods, mechanism, and applications of photodeposition in photocatalysis: a review, Chem. Rev. 116 (2016) 14587–14619.
[112] Y. Wang, C. Sun, X. Zhao, B. Cui, Z. Zeng, A. Wang, G. Liu, H. Cui, The application of nano-TiO_2 photo semiconductors in agriculture, Nanoscale Res. Lett. 11 (2016) 529.
[113] G. Corro, N. Sánchez, U. Pal, S. Cebada, J.L.G. Fierro, Solar-irradiation driven biodiesel production using Cr/SiO_2 photocatalyst exploiting cooperative interaction between Cr^{6+} and Cr^{3+} moieties, Appl. Catal. B 203 (2017) 43–52.
[114] C. Lee, H. Choi, C. Lee, H. Kim, Photocatalytic properties of nano-structured TiO_2 plasma sprayed coating, Surf. Coat. Technol. 173 (2003) 192–200.
[115] P. Evans, D. Sheel, Photoactive and antibacterial TiO_2 thin films on stainless steel, Surf. Coat. Technol. 201 (2007) 9319–9324.
[116] Y. Kubota, T. Shuin, C. Kawasaki, M. Hosaka, H. Kitamura, R. Cai, H. Sakai, K. Hashimoto, A. Fujishima, Photokilling of T-24 human bladder cancer cells with titanium dioxide, Br. J. Cancer Suppl. 70 (1994) 1107.
[117] O.L. Kaliya, E.A. Lukyanets, G.N. Vorozhtsov, Catalysis and photocatalysis by phthalocyanines for technology, ecology and medicine, J. Porphyr. Phthalocya. 3 (1999) 592–610.
[118] H. Chen, C.E. Nanayakkara, V.H. Grassian, Titanium dioxide photocatalysis in atmospheric chemistry, Chem. Rev. 112 (2012) 5919–5948.
[119] Z. Bian, F. Cao, J. Zhu, H. Li, Plant uptake-assisted round-the-clock photocatalysis for complete purification of aquaculture wastewater using sunlight, Environ. Sci. Technol. 49 (2015) 2418–2424.